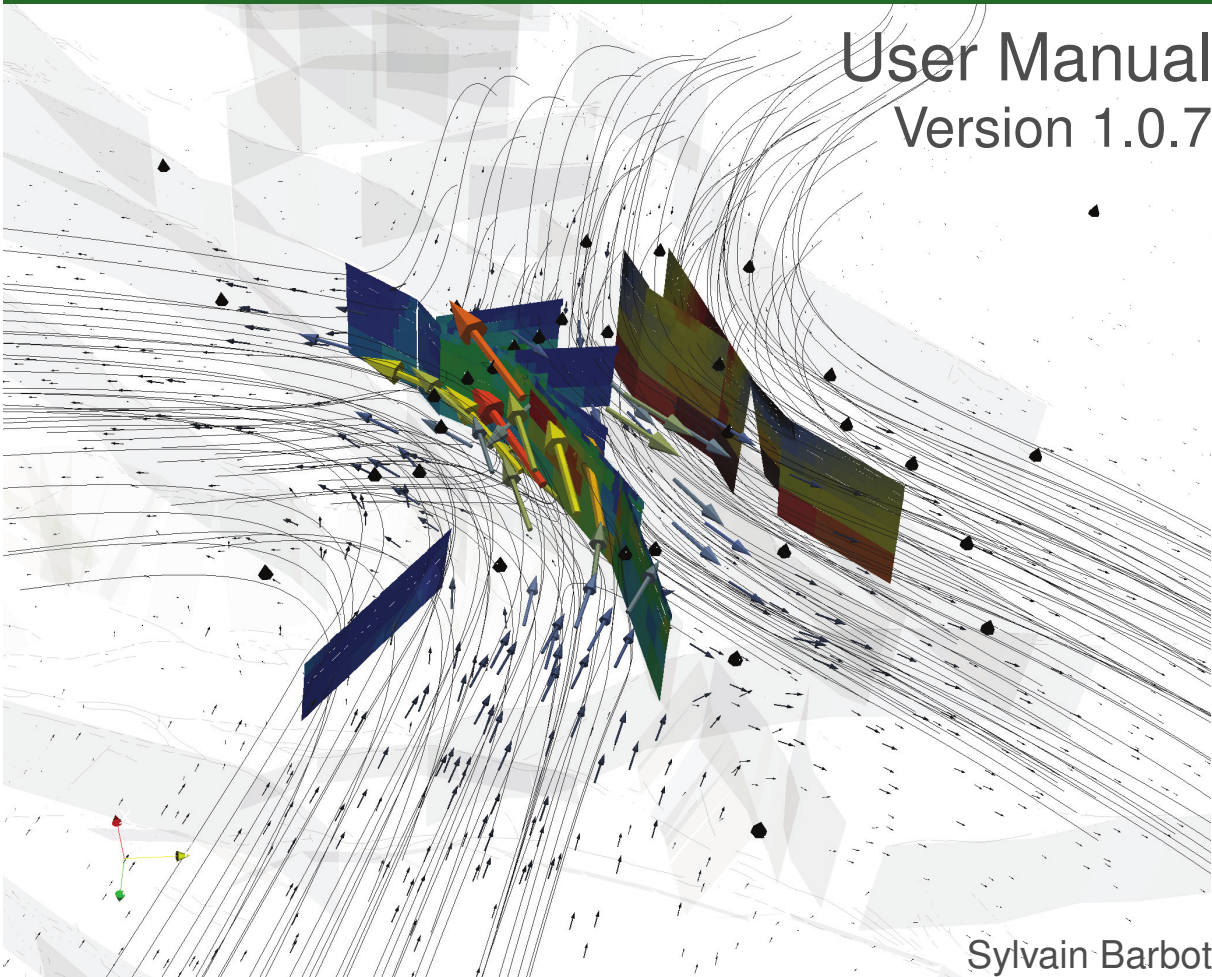


COMPUTATIONAL INFRASTRUCTURE FOR GEODYNAMICS (CIG)

Relax

User Manual
Version 1.0.7



Sylvain Barbot

www.geodynamics.org

Relax: Nonlinear Postseismic Relaxation in the Fourier Domain

User's Manual

Sylvain Barbot (sbarbot@ntu.edu.sg)

Earth Observatory of Singapore, Nanyang Technological University

Oct. 11th, 2011, last revision July. 3rd, 2014

1 Introduction

The open-source program Relax evaluates the displacement and stress in a half space with gravity due to dislocations [e.g., *Okada*, 1992], Mogi sources [*Mogi*, 1958], and surface tractions; and the nonlinear time-dependent deformation that follows due to power-law rheology materials in the bulk and/or rate-strengthening friction faults. The numerical method is based on a Fourier-domain elastic Green's function [*Barbot et al.*, 2009b; *Barbot and Fialko*, 2010a] and an equivalent body-force representation of co-seismic and post-seismic deformation processes [*Barbot et al.*, 2009a; *Barbot and Fialko*, 2010b]. Application of the method for the 2004 Mw 6.0 Parkfield earthquake can be found in the work of *Barbot et al.* [2009a] and *Bruhat et al.* [2011]. A coupled model of afterslip and laterally-heterogeneous viscoelastic flow following the 1999 Mw 7.6 Chi-Chi earthquake using Relax is described by *Rousset et al.* [2012].

The range of applications for the earthquake-cycle modeling include i) co-seismic displacement and Coulomb stress calculation, ii) quasi-static stress transfer between earthquakes due to a postseismic transient, iii) modeling of postseismic transients including nonlinear rheologies and multiple mechanisms, iv) cycle of multiple earthquakes and spin-up models, v) loading cycle of lakes or the monsoon, vi) generation of viscoelastic Green's functions for kinematic inversions of geodetic time series.

2 Acknowledgments

We are thankful for the support of Yuri Fialko during the early development of the methodology at the Institute of Geophysics and Planetary Physics, Scripps Institution of Oceanography. We acknowledge the contribution of Walter Landry, who ensured the portability of the code and streamlined its installation process. We appreciate the efforts of Lucile Bruhat, Yaru Hsu, Mikhail Kogan, Zhen Liu and Baptiste Rousset for testing an earlier version of the code. We are grateful to the work of Sagar Masuti, at the Earth Observatory of Singapore, who ported the code to CUDA. The support of the Computational Infrastructure for Geodynamics is greatly appreciated. Feedback from many users around the world contributed to improving the quality of the software and documentation.

Contents

1	Introduction	1
2	Acknowledgments	1
3	Theoretical background	3
3.1	Green's function	3
3.2	Time integration	4
3.3	Equivalent body-force representation of dislocation	4
4	Setting up the program	6
4.1	Introduction	6
4.2	Running on personal computer	6
4.3	Running on a cluster	7
5	Modeling a deformation scenario	8
5.1	Fault geometry	8
5.2	Depth-dependent constitutive parameters	9
5.3	Lateral variations of viscosity	10
6	Examples	13
6.1	Simple coseismic model	13
6.2	Simple viscoelastic model	16
6.3	Simple afterslip model	19
6.4	Stress change calculations	21
7	Catalogue of published slip distribution models	25
8	post-processing scripts	26
8.1	extrude.sh	26
8.2	flt2vtp.sh	26
8.3	grdmap.sh	26
8.4	grdcoulomb.sh	27
8.5	seg2flt.py	28
9	Outputs	29
10	Benchmarks	31
10.1	Coseismic deformation	31
10.2	Non-linear viscoelastic relaxation	32
11	Using Paraview with Relax	34

The cover image is a Paraview visualization of the displacement field produced by the 1992 Mw 7.3 Landers earthquake from the coseismic slip model of *Fialko* [2004]. The coseismic shear stress on the Hector Mine faults is shown on the far right. The streamlines and the vectors indicate the direction of motion. The shadowed neighboring faults are from UCERF 2 and the prisms indicate continuous GPS stations. The model and the visualization can be reproduced using the material provided in the examples.

3 Theoretical background

3.1 Green's function

The approach used in Relax to evaluate the three-dimensional displacement in a half space is to solve for the displacement field, for static deformation, or the velocity field, for quasi-static problems, using the elastic Green's function. Static deformation caused by earthquakes and time-dependent processes such as viscoelastic flow, poroelastic rebound and fault afterslip can be represented by equivalent body forces and surface tractions so the methods consists, without loss of generality, in finding the displacement and stress caused by an arbitrary distribution of body forces f_i and surface tractions subjected to a mixed boundary condition with buoyancy. Consider the inhomogeneous Navier's equation

$$\mu \left(\frac{\alpha}{1-\alpha} u_{j,ij} + u_{i,jj} \right) + f_i = 0 \quad (1)$$

where μ is the shear modulus, α is a dimensionless parameter that can be expressed in terms of the Lamé's parameters or the Poisson's ratio

$$\alpha = \frac{\lambda + \mu}{\lambda + 2\mu} = \frac{1}{2(1-\nu)}, \quad (2)$$

u_i is the displacement (or velocity) and f_i , the internal body force (or force per unit time), subjected to the surface boundary condition

$$q_i + \sigma_{ij} n_j + \Delta \rho g u_3 n_i = 0, \quad x_3 = 0 \quad (3)$$

with σ_{ij} the Cauchy stress tensor, $n_i = (0, 0, -1)$ the surface normal vector and $q_i(x_1, x_2)$, the prescribed surface traction. The solution displacement that satisfies eq. (1) and (3) can be decomposed into a homogeneous and a particular contribution

$$u_i = u_i^h + u_i^p \quad (4)$$

where the displacement field u_i^h is a solution of the homogeneous Navier's equation

$$\alpha u_{j,ij}^h + (1-\alpha) u_{i,jj}^h = 0 \quad (5)$$

with inhomogeneous surface boundary conditions and the particular solution u^p satisfies eq. (1) regardless of the surface boundary condition. The particular solution can be obtained in the Fourier domain

$$\hat{u}_i^p(k_1, k_2, k_3) = \begin{cases} 0, & k_1 = k_2 = k_3 = 0 \\ \frac{1}{\mu} \frac{(1-\alpha) k_l k_l \delta_{ij} - \alpha k_i k_j}{4\pi^2 (k_l k_l)^2} \hat{f}_j, & \text{otherwise} \end{cases} \quad (6)$$

where the k_i are the wavenumbers and the hats correspond to the Fourier transform of the corresponding variables. The zero wavenumber component of the Fourier solution corresponds to a rigid-body displacement and does not correspond to an elastic deformation. The temporary solution requires the following correction to satisfy the traction boundary condition.

$$\begin{aligned} \hat{u}_1^h(k_1, k_2, x_3) &= \left[-2B_1\beta^2 + \alpha\omega_1(B_1\omega_1 + B_2\omega_2)(1 + \beta x_3) \right. \\ &\quad \left. + \alpha i\omega_1\beta B_3(1 - \alpha^{-1} + \beta x_3) \right] e^{-\beta x_3} \\ \hat{u}_2^h(k_1, k_2, x_3) &= \left[-2B_2\beta^2 + \alpha\omega_2(B_1\omega_1 + B_2\omega_2)(1 + \beta x_3) \right. \\ &\quad \left. + \alpha i\omega_2\beta B_3(1 - \alpha^{-1} + \beta x_3) \right] e^{-\beta x_3} \\ \hat{u}_3^h(k_1, k_2, x_3) &= \alpha\beta^2 \left[i(\omega_1 B_1 + \omega_2 B_2) x_3 \right. \\ &\quad \left. - B_3(\alpha^{-1} + \beta x_3) \right] e^{-\beta x_3} \end{aligned} \quad (7)$$

where we have used $\beta = 2\pi (k_1^2 + k_2^2)^{1/2}$. The values of the B_i are chosen to satisfy the inhomogeneous boundary condition

$$\begin{aligned} B_1(k_1, k_2) &= \frac{\hat{p}_1(k_1, k_2)}{2\mu \beta^3} \\ B_2(k_1, k_2) &= \frac{\hat{p}_2(k_1, k_2)}{2\mu \beta^3} \\ B_3(k_1, k_2) &= \frac{\beta \hat{p}_3(k_1, k_2) - i(1 - \alpha)[\omega_1 \hat{p}_1(k_1, k_2) + \omega_2 \hat{p}_2(k_1, k_2)]}{2\mu \alpha \beta^3 (\beta + \gamma)} \end{aligned} \quad (8)$$

where the effective traction \hat{p}_i incorporates external traction and buoyancy

$$\hat{p}_i(k_1, k_2, x_3 = 0) = \hat{t}_i^p + \Delta \rho g \hat{u}_3^p n_i + \hat{q}_i \quad (9)$$

with

$$\hat{u}_3^p(k_1, k_2, x_3 = 0) = \int_{-\infty}^{\infty} \hat{u}_3^p(k_1, k_2, k_3) dk_3 \quad (10)$$

and

$$\hat{t}_i^p(k_1, k_2) = \mu \int_{-\infty}^{\infty} \left(k_j \hat{u}_i^p + k_i \hat{u}_j^p - \frac{1 - 2\alpha}{1 - \alpha} k_l \hat{u}_l^p \delta_{ij} \right) n_j dk_3 \quad (11)$$

The formulation (7-11) is a solution for the elastic deformation in a homogeneous half space with mixed boundary condition. The solution is evaluated analytically in the Fourier domain and a space-domain solution is obtained with a fast Fourier transform. The advantage is that the performance of the computation scales as $N \log N$, where N is the number of samples in the grid, independently of the number of dislocation. The discrete Fourier transform also introduces periodicity in the solution. In many cases, this is not a desired feature, so the boundaries of the computational domain should be as far as possible from the domain of interest.

3.2 Time integration

The time stepping in Relax is done by linearizing the time advance using the Runge-Kutta numerical integration scheme with an adaptive time steps. For viscoelastic flow and afterslip, the instantaneous strain rate is a function of stress only so that one can write

$$\dot{\epsilon} = f(t, \epsilon) \quad (12)$$

The second-order Runge-Kutta numerical integration to integrate the $y' = f(t, y)$ can be summarized as follows:

$$\begin{aligned} y_{n+1} &= y_n + k_2 \\ k_1 &= h * f(t_n, y_n) \\ k_2 &= h * f(t_n + h, y_n + k_1) \end{aligned} \quad (13)$$

The scheme is second-order accurate, so reducing the time steps help avoiding numerical instabilities.

3.3 Equivalent body-force representation of dislocation

The slip on a finite fault can be represented by a linear combination of force moments and surface tractions [Aki and Richards, 1980]. The method is quite popular in seismology to represent an earthquake as a double-couple point source, but the same representation holds for finite sources. It is possible to express analytically the spatial distribution of body forces and surface traction for a patch of rectangular fault slip. For a vertical rectangular

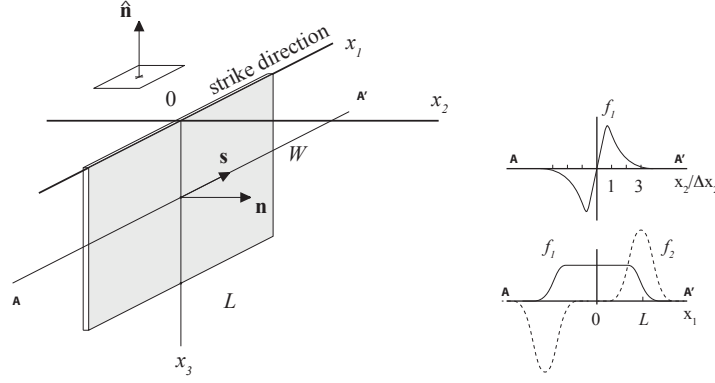


Figure 1: Equivalent body force for a vertical strike-slip fault of length L and width W . The fault slip is tapered with the Ω function of Eq. (15).

strike-slip fault of length L and width W (Figure 1), the body force representation is

$$\begin{aligned} f_1(x_1, x_2, x_3) &= -G \Omega_\beta\left(\frac{x_1}{L}\right) \frac{\partial}{\partial x_2} \delta_T(x_2) \Omega_\beta\left(\frac{x_3}{W}\right) \\ f_2(x_1, x_2, x_3) &= -G \frac{\partial}{\partial x_1} \Omega_\beta\left(\frac{x_1}{L}\right) \delta_T(x_2) \Omega_\beta\left(\frac{x_3}{W}\right) \\ f_3(x_1, x_2, x_3) &= 0 \end{aligned} \quad (14)$$

where the function $\Omega_\beta(x)$ is the tapered boxcar parameterized with roll-off parameter β

$$\Omega_\beta(x) = \begin{cases} 1, & |x| < \frac{1-2\beta}{2(1-\beta)} \\ \cos\left(\pi \frac{(1-\beta)|x| - \frac{1}{2} + \beta}{2\beta}\right)^2, & \frac{1-2\beta}{2(1-\beta)} < |x| < \frac{1}{2(1-\beta)} \\ 0, & \text{otherwise} \end{cases} \quad (15)$$

and the function δ is the numerical equivalent to the Dirac's delta function, for example

$$\delta_T(x) = \frac{1}{T\sqrt{2\pi}} \exp\left(-\frac{x^2}{2T^2}\right) \quad (16)$$

In Relax, the fault thickness is chosen to be the sampling size $T = \Delta x$. A similar relation can be found for faults of arbitrary orientation. The generalization simply involves rotations and translations.

4 Setting up the program

4.1 Introduction

The Relax code is written in Fortran90 with a few I/O functions written in C. The performance of the code depends greatly on the efficiency of the discrete Fourier transform being used. The program can work with the Cooley-Tukey FFT algorithm, for which the source code is provided. For better performance, it is recommended to use the FFT native to the computer environment. The program can readily use the SGI, the FFTW and the Intel MKL FFTs. While we have found that the Intel MKL FFT provides the most efficient calculation, the package provided by the CIG web site implements FFTW.

Both the post-processing and the storage of the simulation are greatly facilitated by writing output files in the cross-platform NetCDF binary format used by the Generic Mapping Tools (GMT). GMT is convenient to rapidly display the simulation results as it is computed, transform the output into other formats or projections (for example, to project the displacement into the Radar line of sight of a satellite to compare with synthetic aperture radar data), make animations and communicate results. Although Relax can output in ASCII format, it is recommended to link the code to the GMT 4.5 libraries. A suite of GMT-based post-processing scripts are available in the `util` directory and require the GMT binaries to be installed in your system.

The output of the simulation can be projected on the fly to geographic coordinates, which is convenient to communicate results to others in a global coordinate system. In Relax, this is performed with the Proj4 library (Proj4.7.1 or higher). It is recommended to install these libraries on your system to facilitate post processing.

Examples input files can be found in the `examples` directory for many earthquakes with published slip distribution models. The directory `examples/tutorials` includes simple directions to evaluate models and carry out post processing and mapping. The man page (type `man relax` in a terminal) provides a thorough description of every input item, and provides additional examples.

4.2 Running on personal computer

The binary packages provided on the CIG website contain everything needed to run simulations. After unpacking the packages, open a terminal (or, in Windows, a Command Prompt) and run the setup script

```
source setup.sh # for Linux and Mac on bash
source setup.csh # for Linux and Mac on csh
setup.bat      # for Windows
```

You should get the response

```
Ready to run Relax.
```

On Linux and Mac, you can check which shell is running (`bash` or `csh`) by typing the command `ps -p $$` in a terminal.

On shared memory machines, such as most modern laptops and desktops, it is possible to run the code in parallel using `openmp`. The number of CPU's used is the maximum number of threads allowed by the machine, or the number found in the environment variable `OMP_NUM_THREADS`. To change the value, type

```
export OMP_NUM_THREADS=4 # for Linux and Mac
set OMP_NUM_THREADS=4    # for Windows
```

on the command line. This command affects all other programs running in this session. On Linux or Mac machines, to set the number for a specific run, prepend the variable definition to your command

```
OMP_NUM_THREADS=4 relax --option
```

Some examples of simple calculations are provided in the `examples/tutorials` directory. For instance, to run the first example, change into the `examples/tutorials` directory and run

```
./run1.sh # for Linux and Mac
./run1.bat # for Windows
```

Alternately, on Windows, you can double-click on `run1.bat` from the file browser.

4.3 Running on a cluster

Relax is programmed to harvest all the cores of a single computer using the OpenMP technology. However, it is not capable of exploiting resources distributed over multiple machines, unlike with MPI. To run the code on a cluster using a queue system, you should allocate only one node at a time, preferably using all the resources. Using PBS, this is accomplished with

```
qsub -l nodes=1:ppn=12 script.sh
```

for machines with 12 cores, where `script.sh` is your Relax script; or by using embedded directives in your script, as follows

```
#!/bin/bash

#PBS -N output_directory
#PBS -q dque
#PBS -l nodes=1:ppn=12
#PBS -l walltime=12:00:00
#PBS -V

if [ "$PBS_O_WORKDIR" != "" ]; then
    echo Working directory is $PBS_O_WORKDIR
    cd $PBS_O_WORKDIR
    echo Running on host `hostname`
    echo Time is `date`
    NPROCS=`wc -l < $PBS_NODEFILE`
    NNODES=`cat $PBS_NODEFILE | uniq | wc -l`
    echo Using $NPROCS cores on $NNODES nodes on machines:
    echo `cat $PBS_NODEFILE`
else
    NPROCS=12
fi

WDIR=./output_directory
if [ ! -e $WDIR ]; then
    echo adding directory $WDIR
    mkdir $WDIR
fi

OMP_NUM_THREADS=$NPROCS relax <<EOF | tee $WDIR/in.param
...
# output directory
$WDIR
...
EOF
```

This script can be executed with the

```
qsub ./script.sh
```

command for queuing, or directly from the terminal with

```
./script.sh
```

for immediate execution, making it versatile for the personal or cluster environments.

5 Modeling a deformation scenario

The computation is performed in a uniform Cartesian grid (see Figure 2). The grid is defined by the number of nodes in the three directions ($SX1$, $SX2$, $SX3$). The code is designed to deal with dimensions that are powers of two only: 128, 256 or 512, for example. The spatial extent of the computational domain depends on the sampling intervals, ($DX1$, $DX2$, $DX3$). The horizontal extent of the computational grid is $SX1 \times DX1$ and $SX2 \times DX2$, in the x_1 and x_2 directions, respectively. In the depth direction, the computational domain extends from 0 to $SX3 \times DX3 / 2$. The coordinate system is right handed, with x_1 pointing north, x_2 pointing east, and x_3 pointing down.

All the parameters that control the simulation in the input file are assumed to be in S.I. units. That is, lengths are in meters (m), slip is in meters (m), time is in seconds (s), the elastic moduli are in Pascals (Pa). The user is responsible for making the choice of parameters self consistent. For earthquake cycle simulations, it is common to use km, MPa and year for distance, stress, and time units, respectively.

To ensure accurate models, the rule of thumb is to have the domain at least ten times the characteristic dimension of the source, or to have any edge of the computational grid about five fault lengths away from a fault tip. Another constraint that ensures good sampling, is to allow for at least five samples per fault. These two constraints can be satisfied simultaneously by maximizing the number of nodes, at the expense of computer memory.

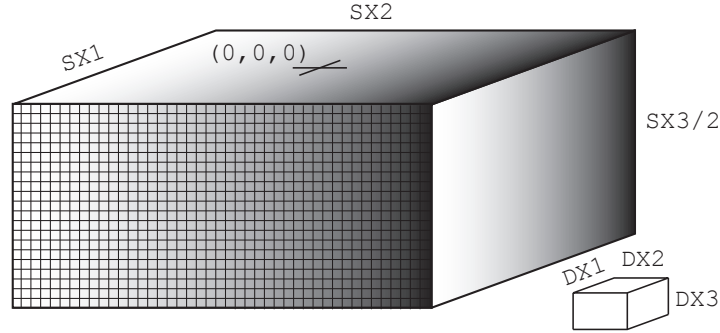


Figure 2: The discretized half space. The origin of the reference system is at the center of the surface. The modeled half space dimension is $-\Delta x_1 \times sx_1/2$ to $\Delta x_1 \times (sx_1 - 1)/2$ in the x_1 direction, $-\Delta x_2 \times sx_2/2$ to $\Delta x_2 \times (sx_2 - 1)/2$ in the x_2 direction and 0 to $\Delta x_3 \times (sx_3 - 1)/2$ in the x_3 (depth) direction.

5.1 Fault geometry

Many simulations imply the relaxation of the stress perturbation from a coseismic rupture. A rupture model consists in a collection of slip patches that discretize the fault geometry and the slip distribution. Every slip patch is described by a geologic representation, as shown in Figure 3. A fault segment is modeled by its length in the along-strike direction, its width in the down-dip direction, the position of the top tip (x_s , y_s , and z_s) and its strike and dip angles. By convention, an observer located at the top fault tip and oriented in the strike direction would face the fault trace and would have the fault dipping to his right for a dip angle between 0° and 90° . This is the same convention used by *Okada* [1992], *Wang et al.* [2003] and *Wang et al.* [2006]. In Relax, to avoid high frequency

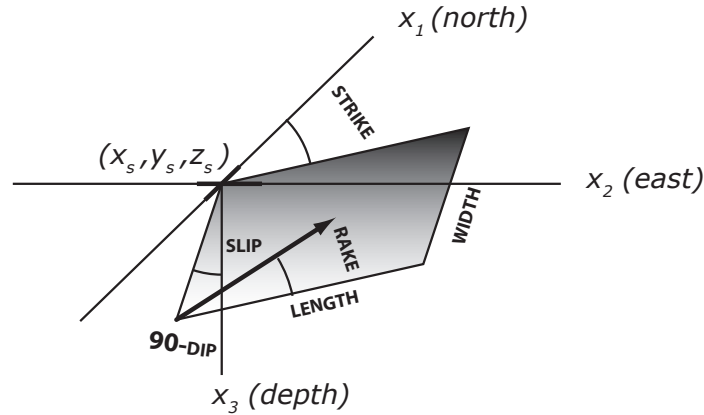


Figure 3: Geologic model of slip on a fault. The fault is described by the position of its top tip, its length in the along-strike direction, width in the down-dip direction, its strike angle and its dip angle. The rake indicates the orientation of slip.

oscillations near a stress concentration (the so-called Gibbs phenomenon), the slip distribution is smoothed near the fault tip. The amplitude of smoothing is controlled by a roll-off parameter going from $\beta = 0$ for no smoothing to $\beta = 0.5$ for strong smoothing. A value of $\beta = 0.2$ ensures stability of the computation. The seismic moment is conserved for all smoothing values. There is a default value of the smoothing parameter defined at the beginning of the input file

```
# dx1,dx2,dx3,beta (0-0.5),nq
0.5 0.5 0.5 0.2 2
```

but it can be amended for each fault patch. In the following excerpt from an input file, all the fault patches use the smoothing parameter $\beta = 0.2$:

```
# no slip  xs      ys      zs length width strike dip  rake
1 1.34 14.2 -45.43 10.0    5.6  4.94 132.7 91 -114.7
2 1.89 10.4 -41.31 10.0    5.6  4.94 132.7 91 -151.8
3 0.46 14.2 -45.41  6.5    3.74  3.53 132.7 91 -150.6
```

but some patches (here, only the second) can be forced to use another value (here, $\beta = 0.5$) as follows:

```
# no slip  xs      ys      zs length width strike dip  rake beta
1 1.34 14.2 -45.43 10.0    5.6  4.94 132.7 91 -114.7
2 1.89 10.4 -41.31 10.0    5.6  4.94 132.7 91 -151.8 0.5
3 0.46 14.2 -45.41  6.5    3.74  3.53 132.7 91 -150.6
```

5.2 Depth-dependent constitutive parameters

The Fourier method used by Relax to solve the displacement field and the quasi-static velocity field implies homogeneous elastic moduli in the half space. However, all other inelastic or physical parameters, such as viscosity, friction properties and stress, can vary arbitrarily in the domain. Relax assumes a background depth dependence for these variables. These properties can be modified locally to simulate slabs, ductile zone, or reproduce the gross features of a geological structure.

Let's look at how to define a viscosity profile for a creme brûlée model, with an elastic plate over a viscoelastic half space. First, note that the Relax input file requires the reference strain rate $\dot{\gamma}_0 = \mu/\eta$, instead of the viscosity η . This is convenient because first, for a purely elastic material, $\dot{\gamma}_0 = 0$, and second, $\dot{\gamma}_0$ is just the reciprocal of the Maxwell relaxation time $t_m = 1/\dot{\gamma}_0$, so one can easily think in terms of time scales of relaxation, instead of viscosities. The default model is elastic, so it is only necessary to indicate where the lithosphere changes from elastic to viscoelastic

```
# number of linear viscous interfaces (where viscosity changes)
1
# no depth gammadot0 cohesion
1 30.0 0.1 0.0
```

Here, we have defined a viscoelastic substrate that extends from 30 km depth down to the bottom of the computational domain. Assuming that the time units are in year, we have define a uniform viscosity giving rise to a Maxwell time $t_m = 1/0.1 = 10$ yr.

Let's look at how to define a viscosity profile for a jelly sandwich model, with a viscoelastic lower crust, a competent, elastic upper mantle, and a viscoelastic asthenosphere. The description of the depth variations of the model is written in a similar way to the PREM model in seismology.

```
# number of linear viscous interfaces for a jelly sandwich strength model
5
# no depth gammadot0 cohesion
1 15.0 0.1 0.0
2 30.0 0.1 0.0
3 30.0 0.0 0.0
4 70.0 0.0 0.0
5 70.0 0.2 0.0
```

Here, the lower crust relaxes with a Maxwell time of $t_m = 10$ yr, and the asthenosphere with a Maxwell time of $t_m = 5$ yr. There is no need to specify the viscosity in the upper 15 km, which is assumed infinite.

5.3 Lateral variations of viscosity

Subducting slabs and shear zones below a transform boundary are examples of major structural elements that introduce lateral variations in viscosity in the lithosphere. Including these elements in the Earth structure is done using ductile zones, which are rectangular regions where the viscosity is modified from the background, depth-dependent, value. The volume where the viscosity changes is defined similarly to a fault (using start position, length, width, strike and dip), but a additional thickness parameter indicates how the volume is extruded from the central plane (Fig. 4).

Let's look at how to define a viscosity profile where the depth of the brittle-ductile transition changes across a geological boundary. We start with an elastic plate overriding a viscoelastic half space with a uniform brittle-ductile transition depth of 15 km with a Maxwell time of $t_m = 1$ yr.

```
...
# number of linear viscous interfaces
1
# no depth gammadot0 cohesion
1 15.0 1 0.0
# number of linear ductile shear zones
1
# no dgammadot0 x1 x2 x3 length width thickness strike dip
1 -1 0 0 10 200 5 200 90 90
...
```

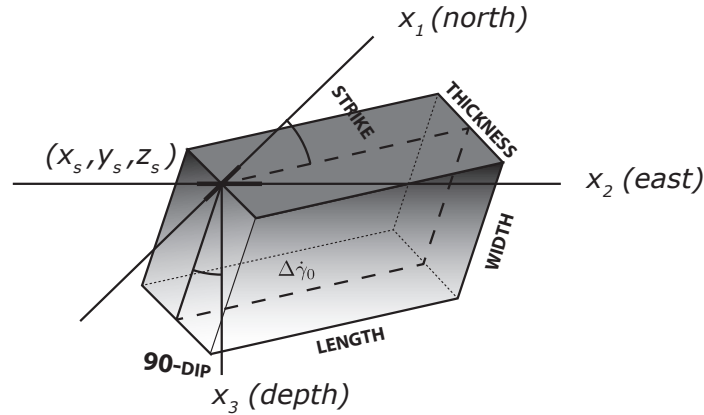


Figure 4: Geometry of a ductile zone anomaly. The ductile zone is described by the position of the tip of the central plane (length in the strike direction, width in the dip direction, strike and dip angles). The thickness parameter indicates how the rectangular volume is extruded from its center plane. The $\Delta\dot{\gamma}_0$ parameter adds to the background value of the fluidity.

We then add a large volume abutting the center of the computational volume, where we modify the fluidity from $\dot{\gamma}_0 = 1 \text{ yr}^{-1}$ to $\dot{\gamma}_0 = 0$, using $\Delta\dot{\gamma}_0 = -1 \text{ yr}^{-1}$. As a null fluidity corresponds to elastic behavior, the brittle-ductile transition occurs 5 km deeper going west to east across the x_1 (north-south) axis. The geometry of a slab can be obtained by modifying the strike and dip angles. Changing the strike of the ductile zone from 90 to 0° would make the transition occur from south to north. If the background and anomalous fluidities add to a negative, unphysical, value, the sum is corrected to null, and the result is an effective elastic property.

Realistic structures can be accounted for from structural data using a large quantity of ductile anomalies tuned to observations. Consider the case of the Sunda subduction slab where the top of the elastic slab is described by a series of fault segments:

#	no	x1	x2	x3	length	width	strike	dip	rake
001	-1008.18345	976.507098	8.540000	50.000	50.094787	-53.2903	3.5252	76.733	
002	-969.881237	944.367717	8.922983	50.000	50.089914	-51.1015	3.4335	78.917	
003	-931.579015	912.228337	9.414930	50.000	50.131393	-50.4005	4.1491	79.626	
004	-893.276793	880.088956	10.365896	50.000	50.219974	-48.2526	5.3646	81.783	
005	-854.974571	847.949576	11.813879	50.000	50.404913	-46.9655	7.2673	83.089	
006	-816.672349	815.810195	11.651879	50.000	50.416558	-46.1198	7.3703	83.930	
007	-778.370126	783.670815	11.301228	50.000	50.406643	-44.0841	7.2827	85.948	
008	-740.067904	751.531434	11.463158	50.000	50.410988	-41.9865	7.3212	88.029	
009	-701.765682	719.392054	11.242973	50.000	50.406957	-40.3630	7.2855	89.639	
010	-663.463460	687.252674	10.615908	50.000	50.373596	-40.3511	6.9824	89.651	
011	-625.161238	655.113293	10.455476	50.000	50.350356	-40.8200	6.7630	89.185	
...									

which is saved in the file `sunda.flt`. A three-dimensional model of the elastic slab can be constructed by extending the fault segments into volumes. Lets consider a 80 km thick slab. We start with a depth-dependent model with visco-elastic relaxation below 80 km:

```
# number of linear viscous interfaces for elastic plate
```

```
1
```



```
# no depth gammadot0 cohesion
1 80.0 1.0 0.0
# number of linear ductile zone
0
```

and let's add the down-going slab:

```
# number of linear viscous interfaces for elastic plate
1
# no depth gammadot0 cohesion
1 80.0 1.0 0.0
# number of linear ductile zone
`grep -v "#" sunda.flt | wc`
# nb dgammadot0 x1 x2 x3 length width thickness strike dip
`grep -v "#" sunda.flt | awk 'print NR,-10,$2,$3,$4,$5,80,$6,$7,$8+90'`
...
```

The last line creates a list of blocks extending the slab interface down and reducing the fluidity by a large number (-10 yr^{-1}) to set the fluidity to 0 and the viscosity to infinity. The slab geometry is shown in Fig. 5.

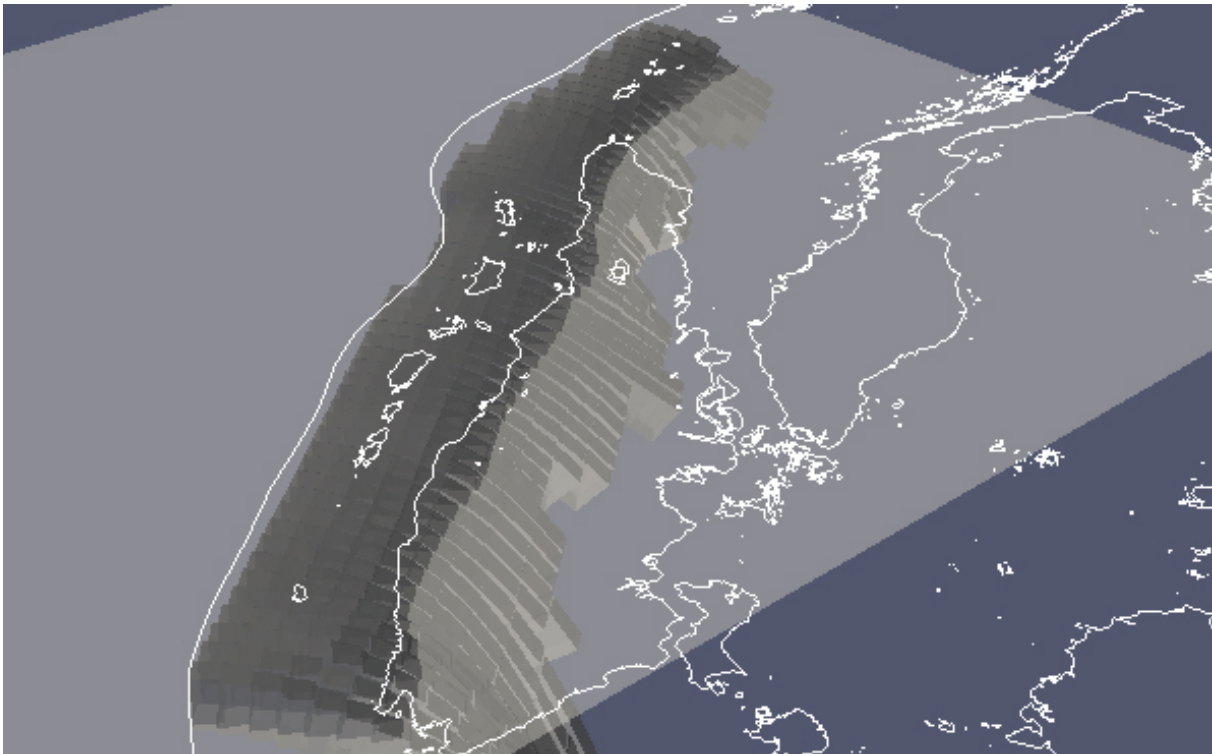


Figure 5: Three-dimensional viscoelastic structure for the Sunda down-going slab. The opaque interface represent an elastic lithosphere extended at depth by the cubic boxes (ductile zones). The mantle wedge is below Sumatra.

6 Examples

6.1 Simple coseismic model

Let's consider first the simplest input model to compute the static deformation due to a left-lateral strike-slip fault. Figure 6 shows the entire input file required to describe the simulation. Note how the code is called, with the command `relax --no-proj-output <<EOF`. In unix, it means that all the text that appears after this line, until the three characters EOF are found, is considered as input for the program. In this case, the program is called with the option `--no-proj-output` to indicate that the output does not have to be projected in lat/lon coordinates. It can be useful to call the program with the `--dry-run` option, i.e.,

```
relax --no-proj-output --dry-run <<EOF
# SX1,SX2,SX3 (grid size)
256 256 256
# dx1,dx2,dx3 (km),beta (0-0.5),nq (2)
0.5 0.5 0.5 0.2 2
...
```

to check the geometry of the model. In this case, all the fault patches, the slip distribution and the spatial extent of the grid are exported in the `.vtp` format, which is a standard 3-D geometry format that can be read with such visualization tools as Paraview (<http://www.paraview.org>).

Unless the `--no-vtk-output` option is used, the program exports the displacement field of the entire computational domain in the VTK Legacy binary format for 3-D visualization. For long time-dependent simulation, this output can consume large amount of disk space and it can be useful to discard it with the `--no-vtk-output` option. The stress field is also exported in this format by default. This is cancelled with `--no-stress-output`, but that option cancels out any stress output in GMT format as well.

The standard output of the program is shown in Figure 7. It repeats the details of the input file and adds information such as the recommended maximum sampling size. After the computation, it also outputs one line corresponding to the first time step. It can be useful to save the standard output of the calculation to document what was computed. To do so, one can use the following unix pipeline

```
ODIR=output_directory
```

```
relax <<EOF --no-proj-output --no-stress-output | tee $ODIR/in.param
# SX1,SX2,SX3 (grid size)
256 256 256
# dx1,dx2,dx3 (km),beta (0-0.5),nq (2)
0.5 0.5 0.5 0.2 2
# origin position & rotation
0 0 0
# observation depths for displacement and for stress
0 5
# output directory
$ODIR
# lambda (MPa), mu (MPa), gamma (1/km)
...
```

To visualize the coseismic displacement at the surface, it is convenient to use the script `grdmap.sh`. The plotting routine `grdmap.sh` provided with the code and numerous other post-processing scripts can be used to analyze the modeled scenario. The unix script `grdmap.sh`, a wrapper around GMT programs, produces map views of any grid but is optimized to work with the three-dimensional output of Relax.

```

relax --no-proj-output <<EOF
# SX1,SX2,SX3 (grid size)
256 256 256
# dx1,dx2,dx3 (km),beta (0-0.5),nq (2)
0.5 0.5 0.5 0.2 2
# origin position & rotation
0 0 0
# observation depths for displacement and for stress
0 5
# output directory (all output written here)
output_directory
# lambda (MPa), mu (MPa), gamma (1/km)
3e4 3e4 8.33e-4
# integration time, time step and scaling
0 -1 1
# number of viscous observation slice
0
# number of observation points
0
# number of Coulomb patches
0
# number of prestress interfaces
0
# number of linear viscous interfaces
0
# number of power-law viscous interfaces
0
# number of friction faults
0
# number of interseismic loading strike-slip and opening
0
0
# number of coseismic events (when slip distribution is prescribed)
1
# number of shear dislocations (strike-slip and dip-slip faults)
1
# no slip  xs ys zs length width strike dip rake
      1      1 -10  0  0      10      10      0  90      0
# number of tensile cracks
0
# number of dilatation sources
0
# number of surface traction
0
EOF

```

Figure 6: Input parameters to compute the coseismic deformation due to a left-lateral strike-slip fault with $L = W = 10$ km. The gravity wavelength is defined as $\gamma = (1 - \nu)\rho g/\mu$ where ν is Poisson's ratio, ρ is the density of the crust and g is the acceleration of gravity. The program provides the displacement field and the stress field in multiple formats.

```

# -----
#       nonlinear postseismic relaxation with Fourier-domain Green function
#       * Intel MKL implementation of the FFT
#       * parallel OpenMP implementation with 016/016 threads
#       * export to GRD format
#       * export to VTK format
#       * export to longitude/latitude text format cancelled (--no-proj-output)
# -----
# grid dimension (sx1,sx2,sx3)
# 256 256 256
# sampling (dx1,dx2,dx3), smoothing (beta, nyquist)
# 5.00E-1 5.00E-1 5.00E-1 2.00E-1 2.00E+0
# origin position (x0,y0) and rotation
# 0.00E+0 0.00E+0 0.00E+0
# observation depth (displacement and stress)
# 0.00E+0 5.00E+0
# output directory
# output_directory (time report: output_directory/time.txt)
# lambda, mu, gamma (gamma = (1 - nu) rho g / mu)
# 3.00E+04 3.00E+04 8.33E-04
# time interval, (positive time step) or (negative skip, scaling)
# 0.00E+0 (output every 001 steps, dt scaled by 1.00E+0)
# number of observation planes
# 0
...
# number of events
# 1
# number of coseismic strike-slip segments
# 1
# -----
# no.      slip      xs      ys      zs  length  width strike  dip  rake
# -----
001  1.00E+0 -1.00E+1  0.00E+0  0.00E+0 1.00E+1 1.00E+1    0.0 90.0  0.0
# -----
# number of coseismic tensile segments
# 0
# number of coseismic dilatation point sources
# 0
# number of surface loads
# 0
# max sampling size (hor.,vert.): 4.00E+0 4.00E+0
# -----
coseismic event 001
I | Dt | tm(ve) | tm(pl) | tm(as) | t/tmax | power | C:E^i |
000* 0.00E+00 0.00E+00 0.00E+00 0.00E+00 0.00E+00/0.00E+00 0.00E+00 3.08E+06

```

Figure 7: Output of the Relax program for the input parameters shown in Figure 6. The Relax output can also serve as an input so it can be useful to save it for documentation purposes and to help reproduce past results.

```
grdmap.sh -b -30/30/-30/30 -p -0.05/0.05/0.001 -v 0.5 \
-u "m" -e erpatch.sh output_directory/000
```

where the `-b` option defines the boundary of the map in the GMT format W/E/S/N, the `-p` option defines the range of the color scale for the vertical displacements, the `-v` option defines the length of the vectors for the horizontal displacement, the `-u` option defines the unit of the color scale, and the `-e` option call the additional script `erpatch.sh` to plot the spatial extent of the fault on the map. The last argument `output_directory/000` refers to the prefix of all GMT binary files associated with the index 000. Any file prefix followed by `-north.grd`, `-east.grd` and `-up.grd` can be used in this manner. To look at an individual file, for example the stress component σ_{12} at 5 km depth, simply use

```
grdmap.sh -b -30/30/-30/30 -p -500/500/1 \
-u "kPa" -e erpatch.sh output_directory/000-s12.grd
```

For this command to work, it is assumed that `grdmap.sh` and `erpatch.sh` are both located in a directory listed in the `$PATH` environment variable, such as `/usr/local/bin`.

The coseismic slip distribution of a real earthquake can be a long and detailed description of the source coming from an inversion of geophysical data. To include these models and conform them to the format required by the Relax program, it is convenient to use other unix tricks, such as `awk`, `wc` and the use of variables, for instance, if the source is described in the file `src.dat`, but the file missing a line counter and the units in meters, one can alter it as follows

```
...
# number of coseismic events
1
# number of shear dislocations
`wc src.dat`
# no slip  xs ys zs length width strike dip rake
`awk ' {BEGIN{s=1e3}{print NR,$1/s,$2/s,$3/s,$4/s,$5/s,$6/s,$7,$8,$9}' src.dat `
# number of tensile cracks
0
# number of dilatation sources
0
# number of surface traction
0
EOF
```

The inclusion of unix commands in the input file allows more complex operations, such as filtering out data, shift, rotation and scaling of models, and others. An example complex coseismic slip distribution for the 1992 Mw 7.3 Landers earthquake can be found in the `examples/mojave` directory.

6.2 Simple viscoelastic model

Let's extend our simple coseismic model to include a viscoelastic relaxation in a substrate below 30 km. To do so, we need to specify a rheology at depth and indicate how long to simulate the relaxation. Relax allows two simultaneous viscoelastic relaxation mechanisms, one from a linear rheology

$$\dot{\gamma}^{\text{linear}} = \dot{\gamma}_0 \frac{\tau}{\mu} \quad (17)$$

where $\dot{\gamma}^{\text{linear}}$ is the amplitude of the linear viscoelastic strain and $\dot{\gamma}_0$ is a reference strain rate; and another from a power-law rheology

$$\dot{\gamma}^{\text{power-law}} = \dot{\gamma}_0 \left(\frac{\tau}{\mu} \right)^n \quad (18)$$

where n is the power exponent (usually in the range $n = 2 - 5$). In this example, we only use the linear rheology. Choosing a viscosity with a Maxwell time of $t_m = 1/\dot{\gamma}_0 = 1$ yr, we want to compute 20 relaxation times with a time step of $\Delta t = 0.1$ yr. This scenario is specified with the following input lines

```
...
# elastic moduli and gravity parameter
3e4 3e4 8.33e-4
# integration time, time step
20 0.1
# number of observation planes
0
# number of observation points
0
# number of Coulomb patches
0
# number of prestress interfaces
0
# number of linear viscous interfaces
1
# no depth gammadot0 cohesion
1 30.0 1.0 0.0
# number of linear ductile zones
0
# number of powerlaw viscous interfaces
0
...
```

Note that the time step asked by the program is only the output time step, that is, at what time to output the result. Internally, an optimal time step is always evaluated and the real time step used for the calculation is the smallest of either the internally evaluated value or the time step required to produce an output every multiple of the required time step. The internally evaluated value is always $\Delta t^{\text{internal}} = t_m/10$. Prescribing the output time step can only reduce the computational time step. Note that as a background viscosity has been established, the program requests so called “ductile zones”, which are finite volumes where the background viscosity is perturbed. These volumes are described similarly to for a fault, but with an extra “thickness” parameter indicating how the volumes extrude from the center plane. The standard output of this simulation looks as follows

```
coseismic event 001
I | Dt | tm(ve) | tm(pl) | tm(as) | t/tmax | power | C:E^i |
000* 0.00E+00 0.00E+00 0.00E+00 0.00E+00 0.00E+00/2.00E+1 0.00E+00 3.08E+06
001* 1.00E-01 1.00E+00 1.00E+07 1.00E+07 1.00E-01/2.00E+1 4.25E+06 3.50E+06
002* 1.00E-01 1.00E+00 1.00E+07 1.00E+07 2.00E-01/2.00E+1 3.92E+06 3.89E+06
003* 1.00E-01 1.00E+00 1.00E+07 1.00E+07 3.00E-01/2.00E+1 3.63E+06 4.26E+06
004* 1.00E-01 1.00E+00 1.00E+07 1.00E+07 4.00E-01/2.00E+1 3.35E+06 4.59E+06
005* 1.00E-01 1.00E+00 1.00E+07 1.00E+07 5.00E-01/2.00E+1 3.10E+06 4.90E+06
006* 1.00E-01 1.00E+00 1.00E+07 1.00E+07 6.00E-01/2.00E+1 2.88E+06 5.19E+06
007* 1.00E-01 1.00E+00 1.00E+07 1.00E+07 7.00E-01/2.00E+1 2.67E+06 5.45E+06
```

```

008* 1.00E-01 1.00E+00 1.00E+07 1.00E+07 8.00E-01/2.00E+1 2.48E+06 5.70E+06
009* 1.00E-01 1.00E+00 1.00E+07 1.00E+07 9.00E-01/2.00E+1 2.31E+06 5.93E+06
010* 1.00E-01 1.00E+00 1.00E+07 1.00E+07 1.00E+00/2.00E+1 2.15E+06 6.14E+06
011* 1.00E-01 1.00E+00 1.00E+07 1.00E+07 1.10E+00/2.00E+1 2.00E+06 6.34E+06
012* 1.00E-01 1.00E+00 1.00E+07 1.00E+07 1.20E+00/2.00E+1 1.87E+06 6.53E+06
013* 1.00E-01 1.00E+00 1.00E+07 1.00E+07 1.30E+00/2.00E+1 1.74E+06 6.70E+06
014* 1.00E-01 1.00E+00 1.00E+07 1.00E+07 1.40E+00/2.00E+1 1.63E+06 6.86E+06
015* 1.00E-01 1.00E+00 1.00E+07 1.00E+07 1.50E+00/2.00E+1 1.53E+06 7.01E+06
016* 1.00E-01 1.00E+00 1.00E+07 1.00E+07 1.60E+00/2.00E+1 1.43E+06 7.15E+06
017* 1.00E-01 1.00E+00 1.00E+07 1.00E+07 1.70E+00/2.00E+1 1.34E+06 7.28E+06
018* 1.00E-01 1.00E+00 1.00E+07 1.00E+07 1.80E+00/2.00E+1 1.26E+06 7.40E+06
019* 1.00E-01 1.00E+00 1.00E+07 1.00E+07 1.90E+00/2.00E+1 1.18E+06 7.52E+06
020* 1.00E-01 1.00E+00 1.00E+07 1.00E+07 2.00E+00/2.00E+1 1.11E+06 7.63E+06
021* 1.00E-01 1.00E+00 1.00E+07 1.00E+07 2.10E+00/2.00E+1 1.05E+06 7.73E+06
022* 1.00E-01 1.00E+00 1.00E+07 1.00E+07 2.20E+00/2.00E+1 9.88E+05 7.82E+06
023* 1.00E-01 1.00E+00 1.00E+07 1.00E+07 2.30E+00/2.00E+1 9.32E+05 7.91E+06
024* 1.00E-01 1.00E+00 1.00E+07 1.00E+07 2.40E+00/2.00E+1 8.79E+05 7.99E+06
025* 1.00E-01 1.00E+00 1.00E+07 1.00E+07 2.50E+00/2.00E+1 8.31E+05 8.07E+06
026* 1.00E-01 1.00E+00 1.00E+07 1.00E+07 2.60E+00/2.00E+1 7.85E+05 8.15E+06
027* 1.00E-01 1.00E+00 1.00E+07 1.00E+07 2.70E+00/2.00E+1 7.43E+05 8.22E+06
028* 1.00E-01 1.00E+00 1.00E+07 1.00E+07 2.80E+00/2.00E+1 7.03E+05 8.28E+06
029* 1.00E-01 1.00E+00 1.00E+07 1.00E+07 2.90E+00/2.00E+1 6.66E+05 8.35E+06
030* 1.00E-01 1.00E+00 1.00E+07 1.00E+07 3.00E+00/2.00E+1 6.31E+05 8.40E+06
031* 1.00E-01 1.00E+00 1.00E+07 1.00E+07 3.10E+00/2.00E+1 5.98E+05 8.46E+06
032* 1.00E-01 1.00E+00 1.00E+07 1.00E+07 3.20E+00/2.00E+1 5.67E+05 8.51E+06
033* 1.00E-01 1.00E+00 1.00E+07 1.00E+07 3.30E+00/2.00E+1 5.39E+05 8.56E+06
034* 1.00E-01 1.00E+00 1.00E+07 1.00E+07 3.40E+00/2.00E+1 5.11E+05 8.61E+06
035* 1.00E-01 1.00E+00 1.00E+07 1.00E+07 3.50E+00/2.00E+1 4.86E+05 8.65E+06
...

```

The standard output indicates the evaluated Maxwell time (if the viscosity is not uniform, the smallest value of the inferred Maxwell time is used) for the viscoelastic rheology, in the `tm(ve)` column. This value should not evolve throughout the calculation. The time step where output is written to disk are shown with an asterisk, such as `014*`. As the output time step corresponds to the computational time step, the value of the displacement, velocity, stress and other variables are output to disk at every time step. The column `power` is important to check the sanity of the calculation. For a relaxation scenario, the power should reduce at each time step. If not the case, it is symptomatic of a numerical integration error. To correct this, decrease the time steps, or the spatial sampling, or both. The last column is the cumulative moment of inelastic deformation and should always increase.

By default, the deformation is written to disk in map view, for mapping with GMT, or in volume, for 3-D rendering with Paraview, at each step. For time dependent problems, it is convenient for certain points in the domain to save the time series of deformation in a single file. To do so, define “observation points” as follows

```

...
# number of observation planes
0
# number of observation points
3
# no name      x1      x2      x3
001 GPS1  1.00E+1  0.00E+0  0.00E+0
002 GPS2  2.00E+1  0.00E+0  0.00E+0
003 GPS3  3.00E+1  0.00E+0  0.00E+0

```

```
# number of stress observation segments
0
...
```

The observation points are given a four-character name `name` and the time series of displacement and stress is listed in the output file `name.txt`. Using the above example, we obtain

```
> more output_directory/GPS1.txt
#          t          u1          u2          u3          s11          s12          s13
0.000E+00 -1.736E-05 1.726E-01 -2.343E-08 1.034E-03 -2.199E+03 4.950E-01
1.000E-01 -1.738E-05 1.726E-01 -2.356E-08 1.035E-03 -2.198E+03 4.950E-01
2.000E-01 -1.739E-05 1.727E-01 -2.368E-08 1.036E-03 -2.197E+03 4.951E-01
3.000E-01 -1.741E-05 1.728E-01 -2.376E-08 1.035E-03 -2.197E+03 4.951E-01
...
```

where we have discarded the last three component of the stress tensor in the interest of space. The observation points list the cumulative displacement and stress, including the initial perturbation from an earthquake and the contribution due to the viscoelastic relaxation.

In many cases, the observation points may be the coordinates of GPS stations in a large network or the ground coordinates of the pixels of a synthetic aperture radar interferogram, or some other image of surface deformation. If the location of the surface points are listed in a file `pos.xy`, one can create as many time series with a command such as

```
...
# number of observation points
`wc pos.xy`
# no name          x1(north)          x2(east)          x3(depth)
`awk '{printf("%d G%03d %f %f 0\n",NR,NR,$2,$1)}' pos.xy`
# number of stress observation segments
0
...
```

which will create files named `G001.txt`, `G002.txt` and so forth, for each point.

6.3 Simple afterslip model

Let's use Relax to simulate the deep afterslip that follows a main shock. To do so, we will add a fault below the rupture and assign rate-strengthening properties. We assume that the slip on the fault is governed by a rate-strengthening constitutive law

$$V = 2\dot{\gamma}_0 \sinh \frac{\Delta\tau}{(a-b)\sigma} \quad (19)$$

where $\Delta\tau$ is the stress perturbation due to the earthquake, which is slowly relaxed, and $(a-b)\sigma$ and $\dot{\gamma}_0$ are constitutive parameters. In general, a good value for $(a-b)\sigma$ is of the order of the stress drop of the earthquake, and perhaps slightly smaller. The dimension-less ratio

$$k = \frac{\Delta\tau}{(a-b)\sigma}, \quad (20)$$

where $\Delta\tau$ is the stress drop, in the range $1 \leq k \leq 7$. Attention, since $\sinh(x) \sim \exp(x)$ for $x \gg 1$, too small a value for $(a-b)\sigma$ will make the evaluation of the velocity challenging. In this case the execution will stop with an error message indicating a diagnostic value of $\Delta\tau$ and of $(a-b)\sigma$. The time scale of the afterslip scales with

$$t_m^{\text{afterslip}} \propto \frac{L}{2\dot{\sigma}_0} \frac{a\sigma}{G} \quad (21)$$

where L is the dimension of the creep area. One can use this scaling relationship to choose the parameters and obtain a reasonable time scale.

An peculiar behavior of this friction law is that the time evolution is non linear, with in some conditions much faster velocities at the early stage of the afterslip transient than at later times. To resolve this numerically, it requires adaptive time steps. To output the simulation at every computational time step, use negative output time steps:

```
...
# integration time, time step and scaling
20 -1 0.5
...
```

In this case, a third argument is needed to modify the internally-evaluated computational time step (here it will be reduced by a half). For example, to output the solution every 10 computational time steps without altering the internal Δt estimate, use

```
...
# integration time, time step and scaling
20 -10 1
...
```

The definition of an afterslip model includes depth-dependent friction properties and the geometry of a receiver fault. To compute the response of afterslip on a deep extension of the rupture defined in the above examples, use

```
...
# number of nonlinear viscous interfaces
0
# number of fault creep interfaces
1
# no depth    gamma0 (a-b)sig friction cohesion
1 0 0.3 1e3 0.6 0
# number of afterslip planes
1
# no  x1 x2 x3 length width strike  dip rake
1 -10 0 11 10 10 0 90 0
# number of inter-seismic strike-slip segments
0
...
```

The standard output reads

```
coseismic event 001
I | Dt | tm(ve) | tm(pl) | tm(as) | t/tmax | power | C:E^i |
000* 0.00E+00 0.00E+00 0.00E+00 0.00E+00 0.00E+00/2.00E+1 0.00E+00 3.08E+06
001* 1.89E-02 1.00E+07 1.00E+07 3.78E-01 1.89E-02/2.00E+1 1.14E+06 3.10E+06
002* 2.76E-02 1.00E+07 1.00E+07 5.53E-01 4.65E-02/2.00E+1 9.47E+05 3.12E+06
003* 2.97E-02 1.00E+07 1.00E+07 5.94E-01 7.62E-02/2.00E+1 8.06E+05 3.15E+06
004* 2.95E-02 1.00E+07 1.00E+07 5.91E-01 1.06E-01/2.00E+1 7.02E+05 3.17E+06
005* 2.94E-02 1.00E+07 1.00E+07 5.88E-01 1.35E-01/2.00E+1 6.22E+05 3.19E+06
006* 2.93E-02 1.00E+07 1.00E+07 5.86E-01 1.64E-01/2.00E+1 5.57E+05 3.20E+06
007* 2.92E-02 1.00E+07 1.00E+07 5.84E-01 1.94E-01/2.00E+1 5.03E+05 3.22E+06
008* 2.91E-02 1.00E+07 1.00E+07 5.82E-01 2.23E-01/2.00E+1 4.57E+05 3.23E+06
009* 2.90E-02 1.00E+07 1.00E+07 5.80E-01 2.52E-01/2.00E+1 4.17E+05 3.24E+06
```

```

010* 2.90E-02 1.00E+07 1.00E+07 5.79E-01 2.81E-01/2.00E+1 3.82E+05 3.25E+06
011* 2.89E-02 1.00E+07 1.00E+07 5.78E-01 3.10E-01/2.00E+1 3.52E+05 3.26E+06
012* 2.88E-02 1.00E+07 1.00E+07 5.77E-01 3.38E-01/2.00E+1 3.25E+05 3.27E+06
013* 2.88E-02 1.00E+07 1.00E+07 5.75E-01 3.67E-01/2.00E+1 3.01E+05 3.28E+06
...

```

and shows a monotonic decrease of the power and a gradual increase of the time steps.

6.4 Stress change calculations

Relax can be used to evaluate the stress change caused by an earthquake or a magmatic intrusion on other faults and structures. There are five ways to look at stress change in Relax: time series at given points, slices, arbitrary cross sections into the domain, three-dimensional visualization in Paraview, and calculation of stress change along an arbitrary number of receiver faults. In addition to providing instantaneous stress change, Relax can provide the time series of stress change due to both the initial source of the deformation and the transient that follows the event.

By default, Relax exports the displacement and stress as a function of time and space in GMT's .grd format. (Stress export can be cancelled with the `--no-stress-output` command-line option.) In the following example, surface displacements and all stress components at a depth of 5 km are exported in the .grd format.

```

relax --no-proj-output <<EOF
# SX1,SX2,SX3 (grid size)
256 256 256
# dx1,dx2,dx3 (km),beta (0-0.5),nq (2)
0.5 0.5 0.5 0.2 2
# origin position & rotation
0 0 0
# observation depths for displacement and for stress
0 5
...

```

Slices of co-seismic stress change at 5 km depth are in the files 000-s11.grd, 000-s12.grd, 000-s13.grd, 000-s22.grd, 000-s23.grd and 000-s33.grd. These files correspond to the σ_{ij} components of the stress tensor. Other components σ_{ji} can be obtained taking advantage of the symmetry of the stress tensor ($\sigma_{ij} = \sigma_{ji}$). Following earthquakes, it can be interesting to evaluate the pore pressure change as it drives poro-elastic rebound. The pore pressure change is a function of the change in confining pressure σ_{kk} , which can be computed as follows using GMT's `grdmath`

```

index=output/000
grdmath ${index}-s{11,22}.grd ADD ${index}-s33.grd ADD = ${index}-skk.grd

```

To better anticipate the extent of the viscoelastic deformation (where will the rocks flow after an earthquake), we can evaluate the norm of the deviatoric stress τ , as it drives viscoelastic flow (eq. 17). The deviatoric stress tensor σ'_{ij} contains no isotropic component, so we can simply compute its diagonal components as follows

```

grdmath ${index}-s11.grd ${index}-skk.grd 3 DIV SUB = ${index}-s11p.grd
grdmath ${index}-s22.grd ${index}-skk.grd 3 DIV SUB = ${index}-s22p.grd
grdmath ${index}-s33.grd ${index}-skk.grd 3 DIV SUB = ${index}-s33p.grd

```

The vigor of viscoelastic flow will be controlled by the norm of the deviatoric stress tensor (eq. 17) and the direction of the flow will be controlled by how the amplitude of stress projects in different directions. The norm of the deviatoric stress can be evaluated as follows

```
grdmath ${index}-s11p.grd 2 POW ${index}-s22p.grd 2 POW ADD ${index}-s33p.grd \
2 POW ADD 2 DIV ${index}-s12.grd 2 POW ADD ${index}-s13.grd 2 POW ADD \
${index}-s23.grd 2 POW ADD SQRT = ${index}-tau.grd
```

For a more subtle look at the dynamics of stress change, we can look at the log of shear stress change (Fig. 8)

```
grdmath ${index}-tau.grd LOG10 = ${index}-log10-tau.grd
```

The files 001-s11.grd, 001-s12.grd, ..., 001-s33.grd contain the total stress change at time step 1, including both the stress change induced by the original event and the stress change induced by the transient that follows. To look at the stress change due to the relaxation alone, we can isolate it as follows:

```
grdmath 001-s12.grd 000-s12.grd SUB = 001-relax-s12.grd
```

To look at stress change in three dimensions, we can open sigma-0000.vtk in Paraview and look at contours of stress components or compute the deviatoric stress change using the Calculator Filter. Another way is to sample the stress along a cross section using an observation plane:

```
...
# elastic moduli and gravity parameter
3e4 3e4 8.33e-4
# integration time, time step
20 -1 1
# number of observation planes
1
# n      x1      x2 x3 length width  strike dip
1  168.5 -438.7  0   1600   160 112.992  90
...
```

The stress components are then exported in GMT's .grd files 000.op001-s11.grd, 000.op001-s12.grd, ..., 000.op001-s33.grd, where the first index 000 is for the time step and op001 is for observation plane 1. All the calculations described above are applicable: just define the new index to `index=output/000.op001` before running `grdmath`. An example application of map view and cross sections of stress change calculations can be found in *Rousset et al. [2012]*.

Cross sections and maps provide a general view of the extent and amplitude of stress change. But it is sometimes useful to look at stress change on receiver faults. This offers the advantage to be able to decompose the stress components in directions relevant to faults: the strike, dip and fault normal directions. Also, receiver faults can have a non planar overall shape, so using receiver faults allows us to follow a complex fault geometry. Receiver faults are defined by their position, dimension, orientation and static coefficient of friction, for example

```
...
# number of stress observation segments
1
# n  x1 x2 x3 length width strike dip friction
1 -10 0 0 20 10 0 90 0.6
...
```

The stress change is calculated at the center of the fault (here that would be 0,0,5). A time series of stress change at the center of the fault can be found in `cfaults-sigma-0001.txt`. In the case of multiple fault segments, each file will contain all components of the stress tensor, the shear and normal components of the traction vector, the strike- and dip-direction components of the traction vector, the fault-normal component of the traction vector and the Coulomb stress change:

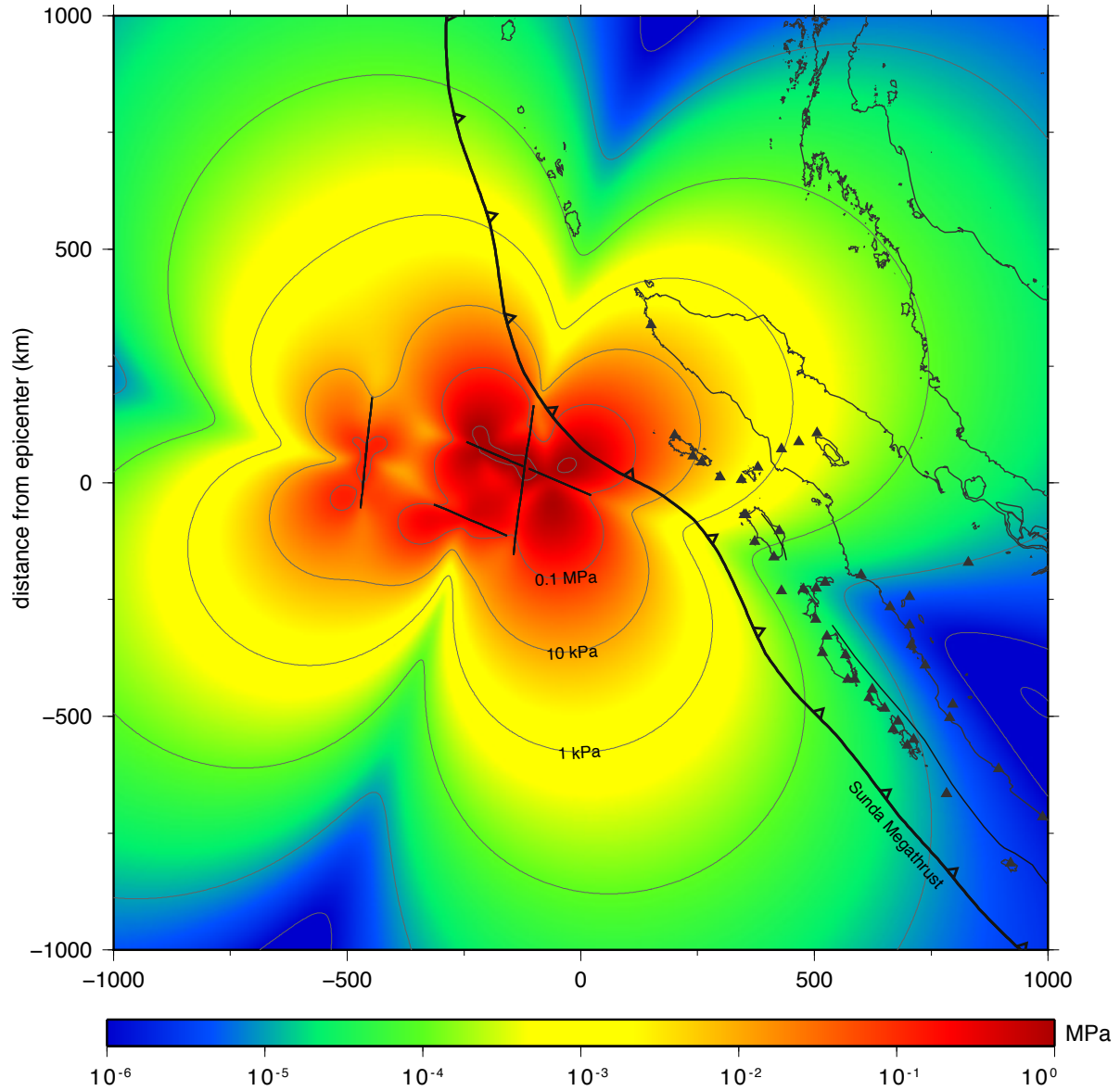


Figure 8: Coseismic stress change at 80 km depth induced by the 2012 Mw 8.6 Wharton Basin earthquake from a slip-distribution model by Hill et al. (2014). The map shows the logarithm of the norm of the deviatoric stress change. The Sunda megathrust around Simulue and Banda Aceh, in northern Sumatra, are experiencing significantly more stress change than other regions.

```
#      t      s11      s12      s13      s22      s23      s33
0.000E+00  2.392E-03  1.583E-03  4.540E-04  4.810E-04  2.366E-04  2.169E-04
```

and

```
      taus      taud      tau      taun      Coulomb
-7.224E-04 -7.665E-04  1.053E-03  4.578E-04  4.707E-02
```

on a single line per time step. The files `rfaults-dsigma-0000.vtp` and `rfaults-dsigma-0000.xy` contain the postseismic stress change on all receiver faults for a given time step for visualization in Paraview and GMT, respectively. The files `rfaults-sigma-0000.vtp` and `rfaults-sigma-0000.xy` contain the cumulative stress change due to both coseismic and postseismic deformation. Together, these files allow us to look at the time series of stress change for a single fault receiver, or look at all the receivers for a given time step. Let's look at an example where we use the same fault as source and receiver:

```
...
# number of stress observation segments
`grep -v "#" slip_model.flt | wc`
# n x1 x2 x3 length width strike dip rake friction
`grep -v "#" slip_model.flt | awk '{ $2=""; $9=0.6; print $0 }'`
# number of prestress interfaces
...
# number of coseismic events
1
# number of shear dislocations (strike-slip and dip-slip faults)
`grep -v "#" slip_model.flt | wc`
# index slip x1 x2 x3 length width strike dip rake
`grep -v "#" slip_model.flt`
```

To define the stress observation plane, we just removed the slip information and added the static friction coefficient to the slip distribution model `slip_model.flt` using `awk`. A convenient way to check the geometry of the stress observation segments is to run `Relax` using the `--dry-run` option. This will output the postseismic stress change on the receiver faults in the file `rfaults-dsigma-0000.vtp` (as this is zero by definition for the 0 time step, this is outputted without actual calculations).

7 Catalogue of published slip distribution models

The directory `examples` contains a large list of input files with published slip distributions of recent earthquakes (Table 1). The database comprises slip distribution for transform boundaries and subduction zones, including all of thrust, strike-slip and normal earthquakes, as illustrated in about 50 examples. New slip distributions will continue to be included and placed in this repository. Authors are encouraged to submit their slip distribution models as they publish their results.

earthquakes	studies
1906 M 7.9 San Francisco	<i>Song et al.</i> [2008]
1964 M 9.2 Alaska	<i>Johnson et al.</i> [1996]
1989 M 6.9 Loma Prieta	<i>Beroza</i> [1991]
1992 Mw 7.3 Landers (California)	<i>Fialko</i> [2004]
1994 Mw 6.3 Northridge (California)	<i>Hudnut et al.</i> [1996]
1999 Mw 7.1 Hector Mine (California)	<i>Simons et al.</i> [2002]
1999 Mw 7.6 Chi-Chi (Taiwan)	<i>Johnson et al.</i> [2001]
2001 Mw 7.8 Kokoxili (Tibet)	<i>Lasserre et al.</i> [2005]; <i>Ryder et al.</i> [2011]
2003 Mw 7.8 Altai	<i>Barbot et al.</i> [2008]
2003 Mw 6.8 Chengkong	<i>Thomas et al.</i> [2014]
2004 Mw 6.0 Parkfield	<i>Bruhat et al.</i> [2011]
2004 Mw 9.1 Sumatra (Indonesia)	<i>Chlieh et al.</i> [2007]
2005 Mw 7.6 Kashmir (Pakistan)	<i>Avouac et al.</i> [2006]
2005 Mw 8.6 Nias (Indonesia)	<i>G. Shao & Chen Ji, UCSB; Konca et al.</i> [2007]
2006 Mw 8.3 Kuril	<i>Steblov et al.</i> [2010]
2007 Mw 7.7 Tocopilla	<i>Béjar-Pizarro et al.</i> [2010]
2008 Mw 7.1 Yutian (Tibet)	<i>Elliot et al.</i> [2010]
2009 Mw 6.3 L'Aquila (Italy)	<i>Atzori et al.</i> [2009]
2010 Mw 6.8 Yushu (Tibet)	<i>Li et al.</i> [2011]
2010 Mw 7.9 Wenchuan (China)	<i>Tong et al.</i> [2011]
2010 Mw 7.2 El Mayor-Cucapah (Mexico)	<i>Wei et al.</i> [2011]
2010 Mw 7.1 Darfield (New Zealand)	<i>Elliot et al.</i> [2012]
2010 Mw 8.8 Maule	<i>Lorito et al.</i> [2011]; <i>Luttrell et al.</i> [2011]
2011 Mw 6.3 Christchurch (New Zealand)	<i>Elliot et al.</i> [2012]
2011 Mw 9.1 Tohoku (Japan)	<i>Wei et al.</i> [2012]; <i>Yamazaki et al.</i> [2011]
2011 Mw 6.9 Tarlay (Myanmar)	<i>Wang, pers. comm.</i> [2013]
2012 Mw 8.6 Wharton Basin	<i>Wei et al.</i> [2013]

Table 1: Table of earthquake slip distribution with validated Relax input files. More slip distributions, Relax input for coseismic deformation and postseismic relaxation simulations, along with geographical information can be found in the `examples` directory.

8 post-processing scripts

8.1 extrude.sh

The script `extrude.sh` computes the coordinates \mathbf{y} of the end points of a fault or fault zone located at \mathbf{x}_0 . Given the length L , the width W and the half thickness T of the fault zone (faults have zero thickness), the end point is at

$$\mathbf{y} = \mathbf{x}_0 + L\hat{\mathbf{s}} + W\hat{\mathbf{d}} + T\hat{\mathbf{n}} \quad (22)$$

The script is useful to create new faults or geometric elements. The script `extrude.sh` reads from the standard input, as follows

```
extrude.sh
#  n    x1    x2    x3 length width thickness strike dip
   1     0     0     0     1     1     0     0  90
+1.000000e+00 -6.123234e-17 -1.000000e+00
```

8.2 flt2vtp.sh

The utility `util/flt2vtp.sh` transforms the slip distribution in the Paraview format for visualization in three dimensions, for example the 1964 M_w 9.2 Alaska slip model in Fig. 9. You can convert single `.flt` files

```
flt2vtp.sh thomas+14_km.flt
```

or a list of files

```
flt2vtp.sh konca+07_km.flt thomas+14_km.flt
```

to create the Paraview files `thomas+14_km.vtp` and `konca+07_km.vtp`. The `.vtp` files contain information to visualize the slip vector, the dip and strike angles. The utility `util/flt2vtp.sh` also works with the standard input,

```
cat konca+07_km.flt | flt2vtp.sh > konca+07_km.vtp
```

This is convenient when you want to merge various input files into one `.flt` file, for example:

```
cat konca+07_km.flt thomas+14_km.flt | flt2vtp.sh > all_faults.vtp
```

8.3 grdmap.sh

To visualize the coseismic displacement at the surface, it is convenient to use the script `grdmap.sh`. The plotting routine `grdmap.sh` provided with the code and numerous other post-processing scripts can be used to analyze the modeled scenario. The unix script `grdmap.sh`, a wrapper around GMT programs, produces map views of any grid but is optimized to work with the three-dimensional output of Relax.

```
grdmap.sh -b -30/30/-30/30 -p -0.05/0.05/0.001 -v 0.5 \
-u "m" -e erpatch.sh output_directory/000
```

where the `-b` option defines the boundary of the map in the GMT format W/E/S/N, the `-p` option defines the range of the color scale for the vertical displacements, the `-v` option defines the length of the vectors for the horizontal displacement, the `"-u"` option defines the unit of the color scale, and the `"-e"` option call the additional script `erpatch.sh` to plot the spatial extent of the fault on the map. The last argument `output_directory/000` refers to the prefix of all GMT binary files associated with the index 000. Any file prefix followed by `-north.grd`, `-east.grd` and `-up.grd` can be used in this manner. To look at an individual file, for example the stress component σ_{12} at 5 km depth, simply use

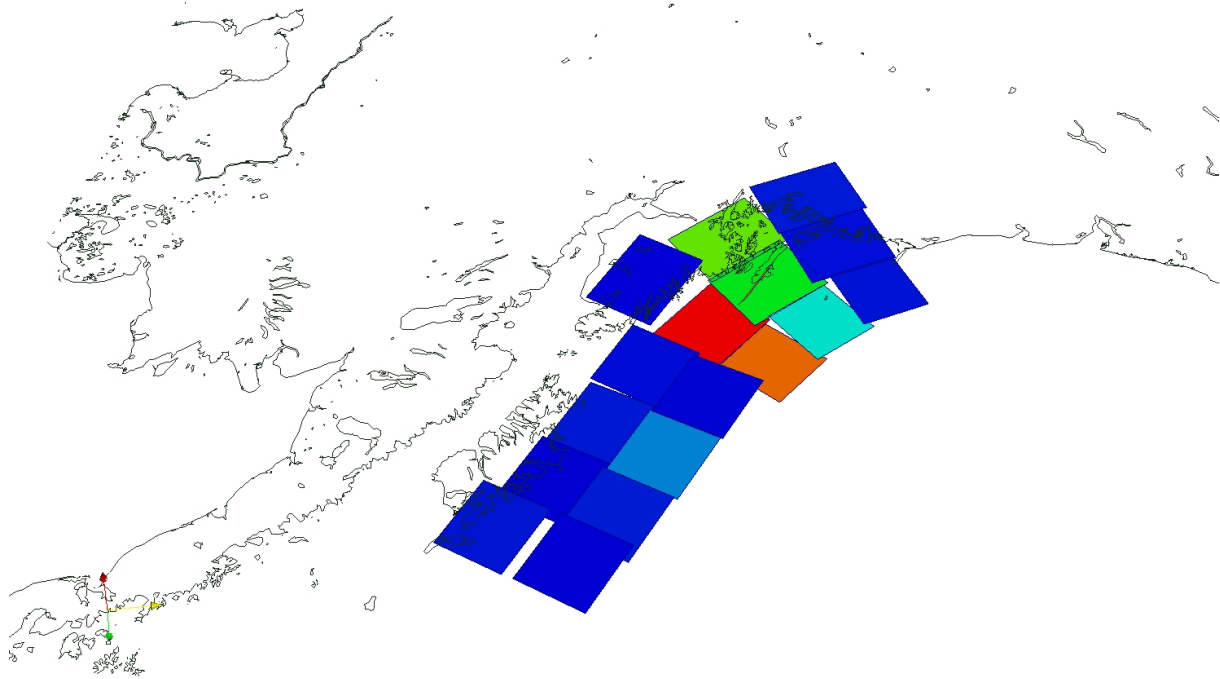


Figure 9: Coseismic slip distribution of the 1964 M_w 9.2 Alaska earthquake [Johnson *et al.*, 1996]. The utility 'flt2vtp.sh' transforms the slip distribution in the Paraview format for visualization in three dimensions.

```
grdmap.sh -b -30/30/-30/30 -p -500/500/1 \
-u "kPa" -e erpatch.sh output_directory/000-s12.grd
```

For this command to work, it is assumed that `grdmap.sh` and `erpatch.sh` are both located in a directory listed in the `$PATH` environment variable, such as `/usr/local/bin`.

8.4 grdcoulomb.sh

The post-processing script `grdcoulomb.sh` projects the stress tensor map produced by Relax into surface tractions and Coulomb stress along a hypothetical fault plane defined by strike and dip orientation and rake angle. For example, to compute the Coulombs stress with a static friction coefficient of $\mu = 0.6$ due to an earthquake on a right-lateral vertical strike-slip fault striking 10° north, use the command

```
grdcoulomb.sh -s 10 -d 90 -r 180 -f 0.6 earthquake/000
```

The calculation assumes that the following files exist: `earthquake/000-s11.grd`, `earthquake/000-s12.grd`, `earthquake/000-s13.grd`, `earthquake/000-s22.grd` and `earthquake/000-s33.grd`. The three components of the traction vectors are expressed in the x_1 , x_2 , x_3 coordinate system and in a fault-centric coordinate system. It provides the strike, dip and normal components of the traction vector. The normal vector of the

receiver fault is

$$\hat{\mathbf{n}} = \begin{pmatrix} -\sin \theta \sin \phi \\ +\cos \theta \sin \phi \\ -\cos \phi \end{pmatrix} \quad (23)$$

The unit strike vector is

$$\hat{\mathbf{s}} = \begin{pmatrix} \cos \theta \\ \sin \theta \\ 0 \end{pmatrix} \quad (24)$$

and the unit dip-direction vector is

$$\hat{\mathbf{d}} = \begin{pmatrix} +\sin \theta \cos \phi \\ -\cos \theta \cos \phi \\ -\sin \phi \end{pmatrix} \quad (25)$$

The unit slip, or Burger's, vector, is $\hat{\mathbf{b}} = \cos r \hat{\mathbf{s}} + \sin r \hat{\mathbf{d}}$. The traction vector in the x1, x2, x3 coordinate system is

$$\hat{\mathbf{t}} = \begin{pmatrix} S_{11}\hat{n}_1 + S_{12}\hat{n}_2 + S_{13}\hat{n}_3 \\ S_{12}\hat{n}_1 + S_{22}\hat{n}_2 + S_{23}\hat{n}_3 \\ S_{13}\hat{n}_1 + S_{23}\hat{n}_2 + S_{33}\hat{n}_3 \end{pmatrix} \quad (26)$$

and the traction vectors in the fault-centric coordinate system are $\mathbf{t}_n = \mathbf{t} \cdot \hat{\mathbf{n}}$, $\mathbf{t}_s = \mathbf{t} \cdot \hat{\mathbf{s}}$, $\mathbf{t}_d = \mathbf{t} \cdot \hat{\mathbf{d}}$. The coulomb stress is $t_c = \mathbf{t} \cdot \hat{\mathbf{b}} + \mu ||\mathbf{t}_n||$. After running `grdcoulomb.sh`, the traction vectors and the Coulomb stress can be visualized using `grdmap.sh`, for example

```
grdmap.sh earthquake/000-tc.grd
```

8.5 seg2flt.py

The Python script `seg2flt.py` converts a segment definition to finely sampled fault file. The script expect a list of index, x1, x2, x3, length, width, strike dip, rake, delta length, delta width, algebraic factor for length, algebraic factor for width. The segment will be cut in small patches of dimension delta length \times delta width. The algebraic factors correspond to a geometric increase of the patches length and width with depth. Use algebraic factors of 1 for a uniform length and width. For example, to create four uniform patches out a segment definition, use

```
echo 1 0 0 0 10 10 45 90 0 5 5 1 1 | seg2flt.py
#  n      x1      x2      x3    length    width    strike    dip    rake
  1      0.0000    0.0000    0.0000    5.0000    5.0000    45.00    90.00    0.0
  2      3.5355    3.5355    0.0000    5.0000    5.0000    45.00    90.00    0.0
  3     -0.0000    0.0000    5.0000    5.0000    5.0000    45.00    90.00    0.0
  4      3.5355    3.5355    5.0000    5.0000    5.0000    45.00    90.00    0.0
```

or to create two shallow patches and a long deep patch, use

```
echo 1 0 0 0 10 10 45 90 0 5 5 2 2 | seg2flt.py
#  n      x1      x2      x3    length    width    strike    dip    rake
  1      0.0000    0.0000    0.0000    5.0000    5.0000    45.00    90.00    0.0
  2      3.5355    3.5355    0.0000    5.0000    5.0000    45.00    90.00    0.0
  3     -0.0000    0.0000    5.0000   10.0000    5.0000    45.00    90.00    0.0
```

This is useful to create observation planes on the fly, from a simple large-scale definition of the fault segment.

The script can also be used to resample slip distributions, for example

```
echo 1 1 0 0 0 10 10 45 90 0 5 5 1 1 | seg2flt.py --with-slip
#  n    slip      x1      x2      x3    length    width    strike    dip    rake
  1 +1.0e+0    0.0000    0.0000    0.0000    5.000    5.000    45.00    90.00    0.0
  2 +1.0e+0    3.5355    3.5355    0.0000    5.000    5.000    45.00    90.00    0.0
  3 +1.0e+0   -0.0000    0.0000    5.0000    5.000    5.000    45.00    90.00    0.0
  4 +1.0e+0    3.5355    3.5355    5.0000    5.000    5.000    45.00    90.00    0.0
```

Combined with `flt2vtp.sh`, this can be used to test the geometry of slip distribution models, for example

```
echo 1 1 0 0 0 10 10 45 90 0 5 5 1 1 | \
    seg2flt.py --with-slip | flt2vtp.sh > test.vtp
```

Used in combination with `extrude.sh`, the script `seg2flt.py` can be used to rapidly create slip distribution and observation planes for geometrically complex fault systems.

9 Outputs

All GMT output files related to a specific time step are prefixed by the index number, for instance `000-east.grd` is the map view of the east component of deformation for index 0. For each time step, for example index 14, one can find

<code>014-north.grd</code>	map view of the north component of cumulative displacement
<code>014-east.grd</code>	map view of the east component of cumulative displacement
<code>014-up.grd</code>	map view of the vertical component of cumulative displacement
<code>014-relax-north.grd</code>	map view of the north component of postseismic displacement
<code>014-relax-east.grd</code>	map view of the east component of postseismic displacement
<code>014-relax-up.grd</code>	map view of the vertical component of postseismic displacement
<code>014-s11.grd</code>	map view of the σ_{11} component of cumulative stress
<code>014-s12.grd</code>	map view of the σ_{12} component of cumulative stress
<code>014-s13.grd</code>	map view of the σ_{13} component of cumulative stress
<code>014-s22.grd</code>	map view of the σ_{22} component of cumulative stress
<code>014-s23.grd</code>	map view of the σ_{23} component of cumulative stress
<code>014-s33.grd</code>	map view of the σ_{33} component of cumulative stress

The export to files in the GMT binary format `.grd` can be cancelled for the interest of space with the `--no-grd-output` option.

All VTK output files for visualization in Paraview are suffixed with the output index numbers, for example `sigma-0014.vtk`. For each time step, for instance index 14, one can find

<code>disp-0014.vtk</code>	subsamped volume of displacement vector
<code>vel-0014.vtk</code>	subsamped volume of velocity vector
<code>sigma-0014.vtk</code>	subsamped volume of stress tensor
<code>power-0014.vtk</code>	subsamped volume of power tensor
<code>disp-relax-0014.vtk</code>	subsamped volume of the relaxation part of the displacement vector (no coseismic)

The output `disp-relax-????.vtk` are only available with the `--with-vtk-relax-output` option. The export to files in the VTK binary format `.vtk` can be cancelled for the interest of space with the `--no-vtk-output` option.

Some other files only contain geometrical information, such as geometry of fault patches, grid dimension, position of observation points:

<code>opts.dat</code>	list of observation points (coordinates and names)
<code>rfaults-001.xy</code>	GMT file containing the slip distribution of event 1
<code>rfaults-001.vtp</code>	Paraview file containing the slip distribution of event 1
<code>rfaults-dsigma-0014.vtp</code>	Paraview file containing the postseismic Coulomb stress for time step 14
<code>rfaults-sigma-0014.vtp</code>	Paraview file containing the Coulomb stress for time step 14
<code>aplane-0001.vtp</code>	Paraview file for the afterslip plane number 1
<code>linearlayer-001.vtp</code>	Paraview file for depth of the first linear viscosity change
<code>cgrid.vtp</code>	Paraview file for extent of the computational domain
<code>weakzones-linear.vtp</code>	Paraview file for all linear ductile zones
<code>weakzones-nonlinear.vtp</code>	Paraview file for all nonlinear ductile zones
<code>time.txt</code>	time associated with time step

The time series of stress and displacement for observation points are in files `NAME.txt`.

10 Benchmarks

The numerical solution produced by Relax has been compared to many other analytical and numerical solutions. Here, we show two examples for static and time-dependent deformation. In general, it is a good practice to setup simulations using the most resource possible (the largest meshes, the smallest sampling).

10.1 Coseismic deformation

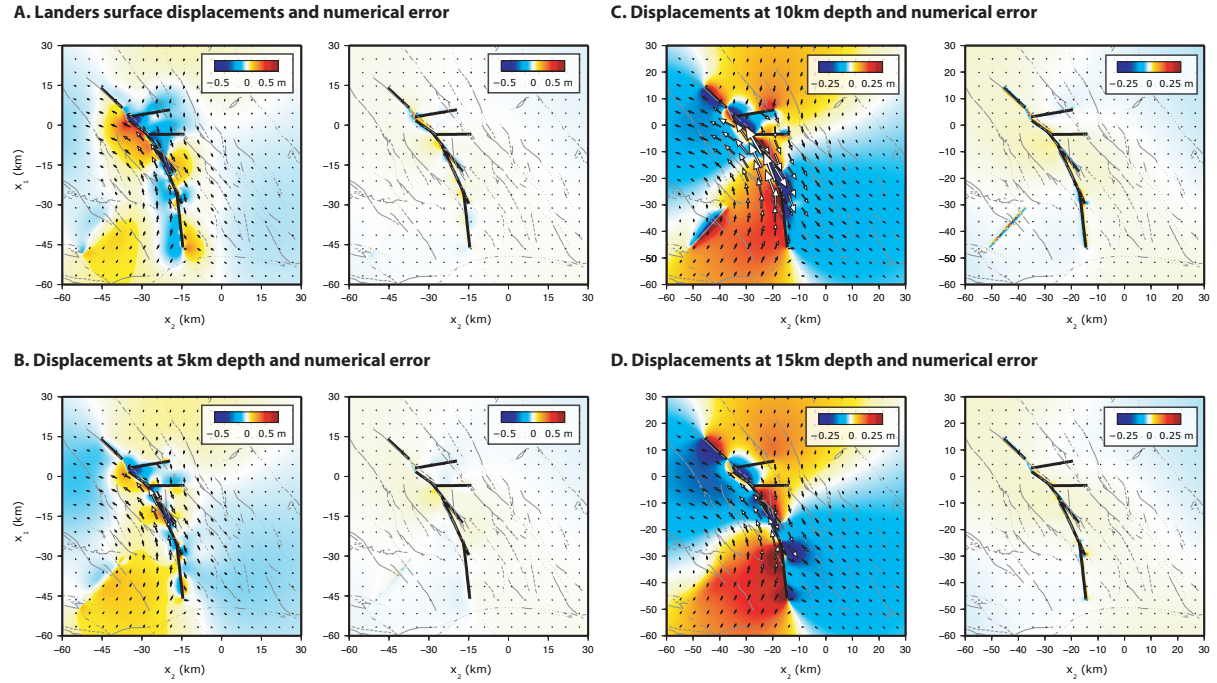


Figure 10: Simulation of the 1992 Mw 7.3 Landers, CA earthquake. Comparison between the Relax numerical solution and the solution obtained with the *Okada* [1992] Green's function at the surface (A), and at 5 km (B), 10 km (C) and 15 km depth (D). For each depth the Relax solution is shown (left) and the residuals with *Okada* [1992]. The arrows indicate horizontal displacement and the color represent vertical displacement (positive up).

Let's consider the coseismic deformation caused by the 1992 Mw 7.3 Landers, CA earthquake. Let's use the slip distribution of [Fialko, 2004], which consists in 426 slip patches

```
...
# number of shear dislocations
426
# index slip x1 x2 x3 length width strike dip rake
1 1.3475 14.246 -45.439 10.056 5.6 4.94 132.7 91.0 -114.7
2 1.8921 10.446 -41.319 10.056 5.6 4.94 132.7 91.0 -151.8
3 0.46688 14.201 -45.481 6.5269 3.74 3.53 132.7 91.0 -150.6
4 0.38986 11.668 -42.734 6.5269 3.74 3.53 132.7 91.0 -175.6
5 1.3331 9.1346 -39.987 6.5269 3.74 3.53 132.7 91.0 172.8
...
```

The corresponding input file can be found in the `examples` directory in the file `landers.sh`. Figure 10 shows the comparison between the calculation with Relax on a 512^3 grid with a sampling of $\Delta x = 0.6$ km and the analytic solution obtained with the *Okada* [1992] Green’s function at various depths. The residuals maps reveals some numerical errors in the near field of the rupture caused by the equivalent body-force representation. Some long wavelength error appear at depth (10c,d) caused by the periodicity of the numerical solution due to the Fourier transform method. Overall the residuals are very small, demonstrating the possibility to model accurately geometrically complex earthquake ruptures.

10.2 Non-linear viscoelastic relaxation

Let’s look at the postseismic relaxation due to the stress perturbation caused by dip-slip faulting, assuming uniform and isotropic elastic properties for a Poisson’s solid (the Lamé parameters are such that $\lambda = G$ and Poisson’s ratio is $\nu = 1/4$). The fault slips 1 m uniformly from the surface to a depth of 10 km and is 40 km long. We consider the case of a nonlinear viscoelastic upper mantle governed by the power-law rheology with $n = 2$. We perform the computation with Relax in a 512^3 grid with a uniform sampling of $\Delta x = 0.8$ km. A snapshot of the surface displacement early in the postseismic transient is shown in Figure 11a. The vertical postseismic displacement has the same polarity as the coseismic displacement. Horizontal postseismic displacements, however, are directed opposite to the coseismic ones. We performed the same simulation using the finite-element software Abaqus and the residuals are shown in the right panel of Figure 11a. The time series of surface postseismic displacements at points numbered from 1 to 8 in the maps are shown in Figure 11b. There is an excellent agreement between the semi-analytic and the finite-element results. The time series are characterized by two striking features. First, initial postseismic velocities are much higher than at later times, as most visible for points 1 and 2. Second, a change in polarity occurs at far-field locations. The change of postseismic displacement orientation is most flagrant for point 6 in the East-West direction. A mild change of polarity can be misleadingly interpreted as a delayed postseismic transient, as for the vertical displacement of point 8, for example.

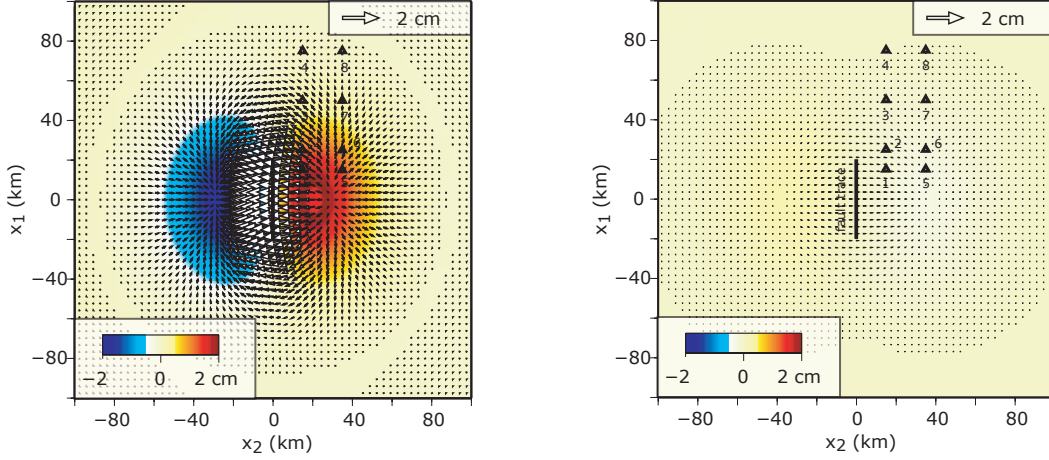
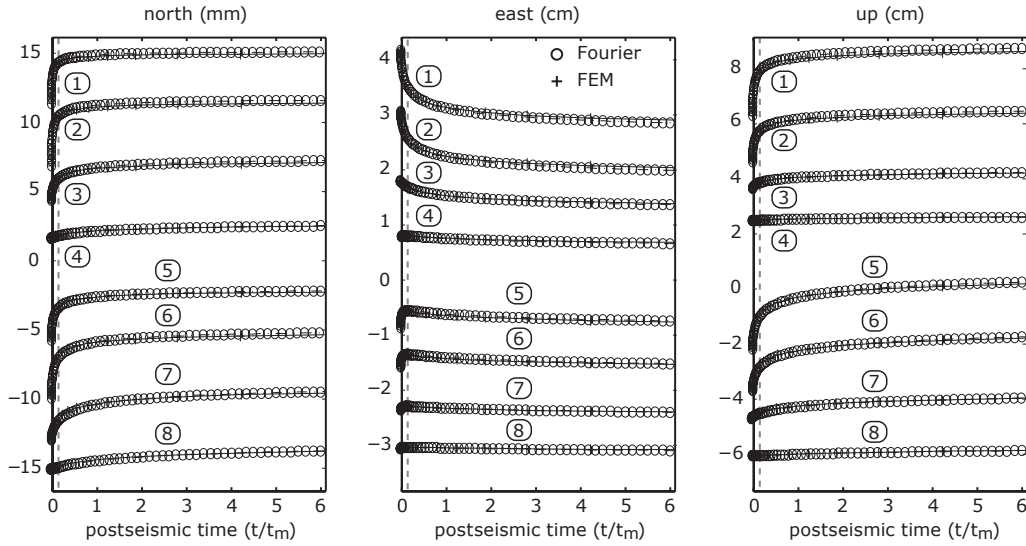
A. Dip-Slip Fault. Powerlaw viscoelasticity ($n=2$). Displacements and residuals with finite-element calculations**B. Comparison between finite-element and Fourier-domain postseismic time series**

Figure 11: Benchmark for time series of surface displacement due to a stress perturbation caused by a dip-slip fault in an elastic plate overriding a nonlinear viscoelastic half space. A vertical dip-slip fault 40 km long extending from the surface to a depth of 10 km slips 1 m. The brittle-ductile transition occurs at a depth of 30 km. The postseismic flow is governed by a power-law rheology with stress exponent $n = 2.0$. Elastic properties are uniform with $\nu = 1/4$. A) A map view of postseismic surface displacements after ten months. A similar computation is performed using finite elements with Abaqus and the residuals are shown in the right panel. B) Time series of surface displacements for the points numbered from 1 to 8 in the corresponding map. The smaller time steps near the onset of the postseismic transient are due to the adaptive time-step procedure. Results from our approach are shown every 5 computation steps for clarity. The residuals between results from our numerical approach and the finite element calculation are less than 5% and show reasonable agreement both in map view and in time.

11 Using Paraview with Relax

This section offers a short introduction to using Paraview to visualize three-dimensional objects and simulations. Paraview also offers a convenient way to check the geometry of the models, including the input slip models and the relative position of other boundaries (viscous layers, ductile zone anomalies, receiver stress faults for Coulomb stress calculation).

The first example uses the output created by the Coulomb stress calculation in the `examples/mojave` directory. To run the example, type

```
cd examples/mojave
./coulomb.sh
```

in a terminal. You can interrupt the program after this line appears

```
coseismic event 001
I | Dt | tm(ve) | tm(pl) | tm(as) | t/tmax | power | C:E^i |
000* 0.00E+00 0.00E+00 0.00E+00 0.00E+00 0.00E+00/2.00E+1 0.00E+00 3.60E+03
```

as we only need the coseismic model. Figures 12 to 15 show the procedure to import and visualize the model. First, load the computational extent of the model (Figs. 12 and 13). Then, load the source patches of the deformation (Fig. 14). Use the `Rescale to Data Range and/or Edit Color Map...` controls in the `Display` tab, if necessary. When running your first models, these first steps are a good way to verify the accuracy of the input geometry. Lastly, load the receiver faults and adjust the color scale (Fig. 15). The stress calculation includes several projections of the stress tensor at the receiver fault location, including normal, shear and Coulomb stress, shear stress in the strike and dip direction, and the full stress tensor. Additional post-processing calculations can be done with the `Calculator` filter.

The second example uses a model of the viscoelastic relaxation that follows the 1992 Mw 7.3 Landers earthquake. To run the simulation with the Paraview output, type

```
./landers.sh --with-vtk-output --with-vtk-relax-output
```

The first option, `--with-vtk-output`, enforces the output in `vtk` format, which is cancelled in `landers.sh`; the second option, `--with-vtk-relax-output` exports the relaxation contribution for three-dimensional visualization. The relaxation contribution is the total deformation, both elastic and viscoelastic, minus the coseismic deformation. This example also produces the output of the first one, so it is possible to reproduce the same steps. Additionally, you can load the three-dimensional coseismic displacement field (`disp-..vtk`), and create the vector field using the `Glyph` filter (Figs. 16 and 17). To look at the relaxation component, load `disp-relax-..vtk`. You can then directly create a vector field, or you can decimate the data set to make the plot less dense (Fig. 18). To plot the postseismic vector field, it is more convenient to move to another time step (postseismic component is zero by definition at time step zero). You can then apply the `Glyph` filter on the data subset (Fig. 19). Finally, you can load the California faults trace or the UCERF three-dimensional fault model using the ancillary files located in `examples/mojave/paraview`.

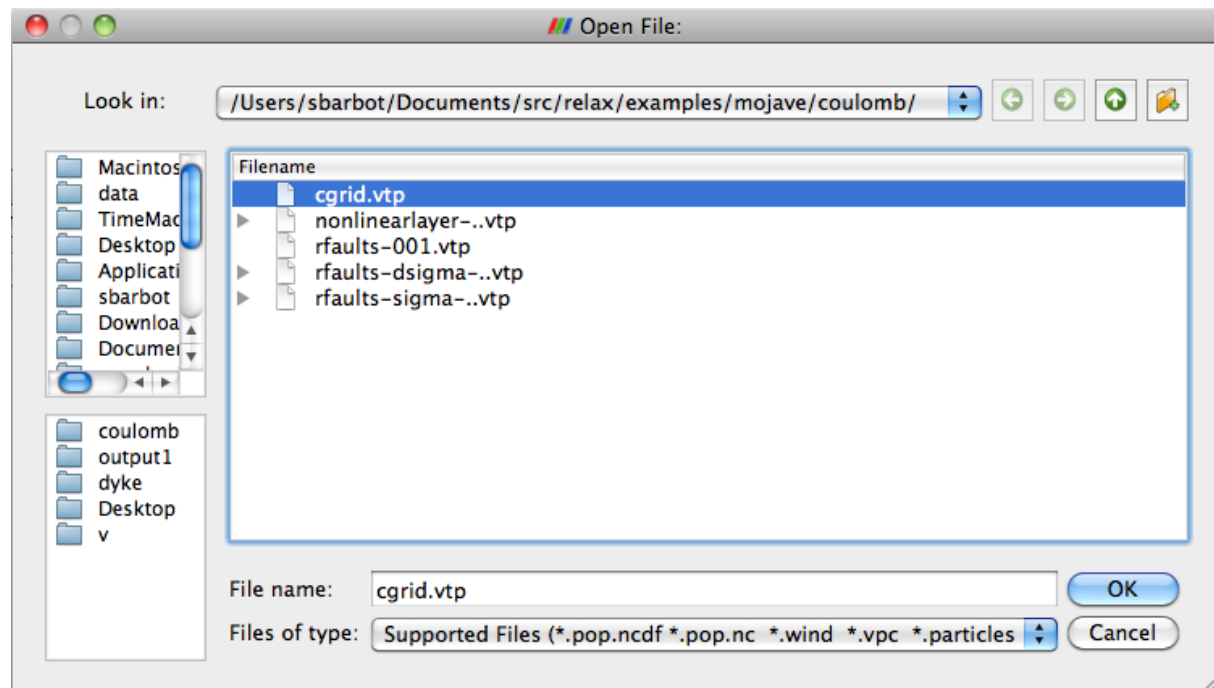


Figure 12: Open the file containing the spatial extent of the computational domain.

References

- Aki, K., and P. G. Richards, *Quantitative Seismology*, vol. I, W. H. Freeman and company, New York, 1980.
- Atzori, S., et al., Finite fault inversion of DInSAR coseismic displacement of the 2009 L'Aquila earthquake (central Italy), *Geophys. J. Int.*, 36(15), 2009.
- Avouac, J.-P., F. Ayoub, S. Leprince, O. Konca, and D. V. Helmberger, The 2005, Mw 7.6 Kashmir earthquake: Sub-pixel correlation of ASTER images and seismic waveforms analysis, *Earth. Plan. Sc. Let.*, 249(3-4), 514?528, 2006.
- Barbot, S., and Y. Fialko, Fourier-domain Green's function for an elastic semi-infinite solid under gravity, with applications to earthquake and volcano deformation, *Geophys. J. Int.*, 182(2), 568–582, doi:10.1111/j.1365-246X.2010.04655.x, 2010a.
- Barbot, S., and Y. Fialko, A unified continuum representation of postseismic relaxation mechanisms: semi-analytic models of afterslip, poroelastic rebound and viscoelastic flow, *Geophys. J. Int.*, 182(3), 1124–1140, doi:10.1111/j.1365-246X.2010.04678.x, 2010b.
- Barbot, S., Y. Hamiel, and Y. Fialko, Space geodetic investigation of the coseismic and postseismic deformation due to the 2003 Mw 7.2 Altai earthquake: Implications for the local lithospheric rheology, *J. Geophys. Res.*, 113(B03403), doi:10.1029/2007JB005063, 2008.
- Barbot, S., Y. Fialko, and Y. Bock, Postseismic Deformation due to the Mw 6.0 2004 Parkfield Earthquake: Stress-Driven Creep on a Fault with Spatially Variable Rate-and-State Friction Parameters, *J. Geophys. Res.*, 114(B07405), doi:10.1029/2008JB005748, 2009a.

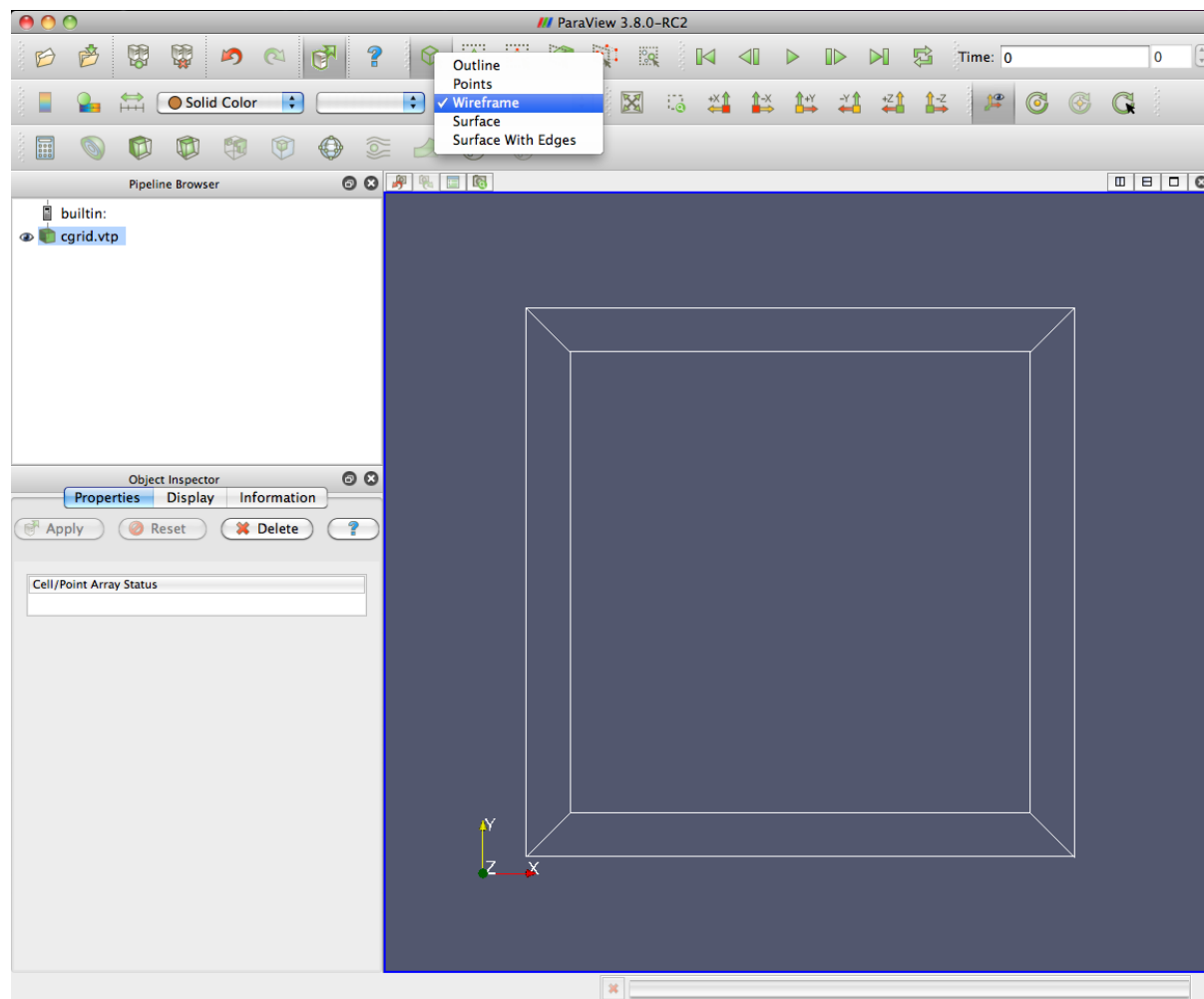


Figure 13: Change the representation to wireframe to display online the boundary of the rectangular volume.

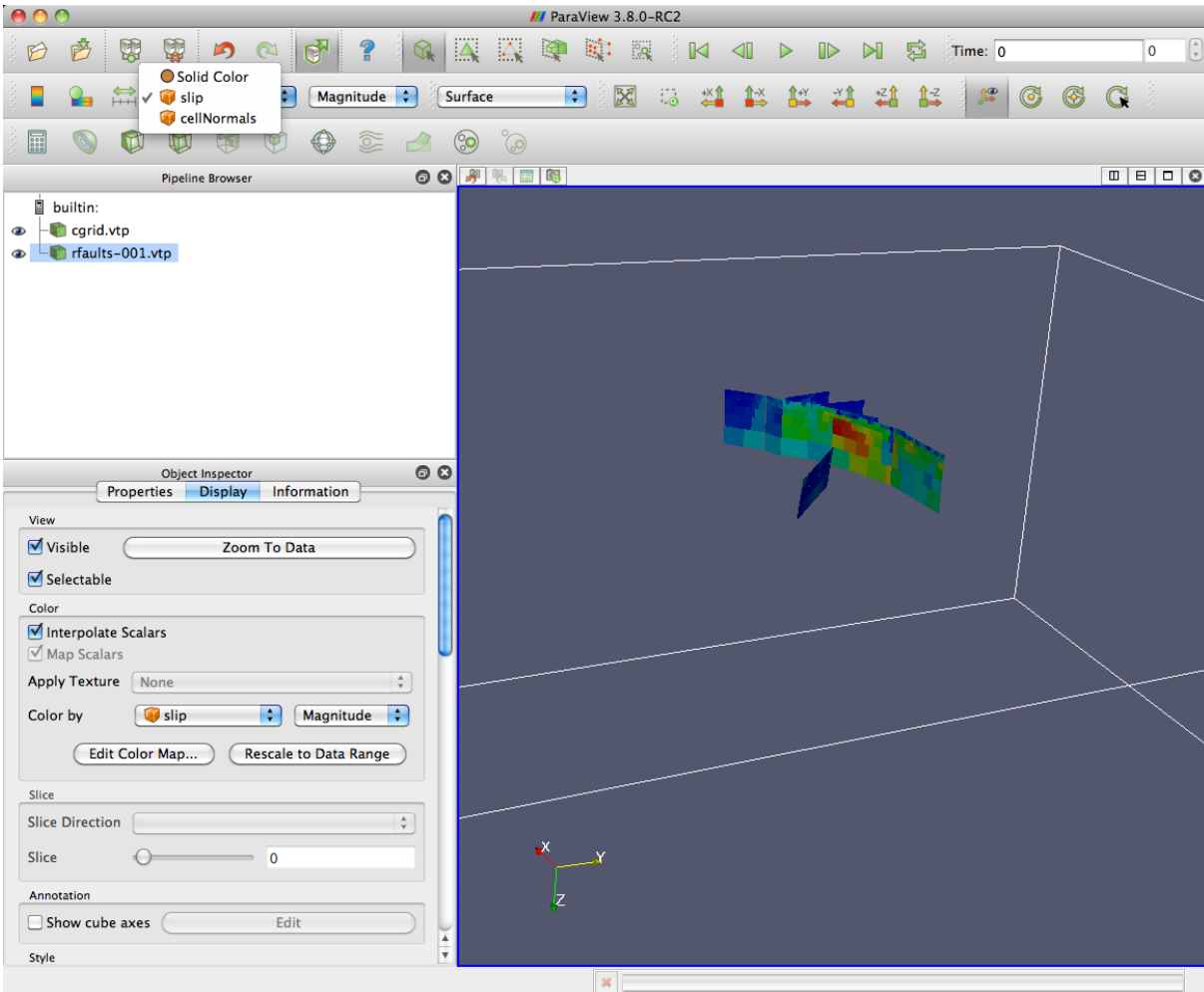


Figure 14: Load the Landers slip model and color by the amplitude of slip. Rescale to data range in the “display” menu, if necessary.

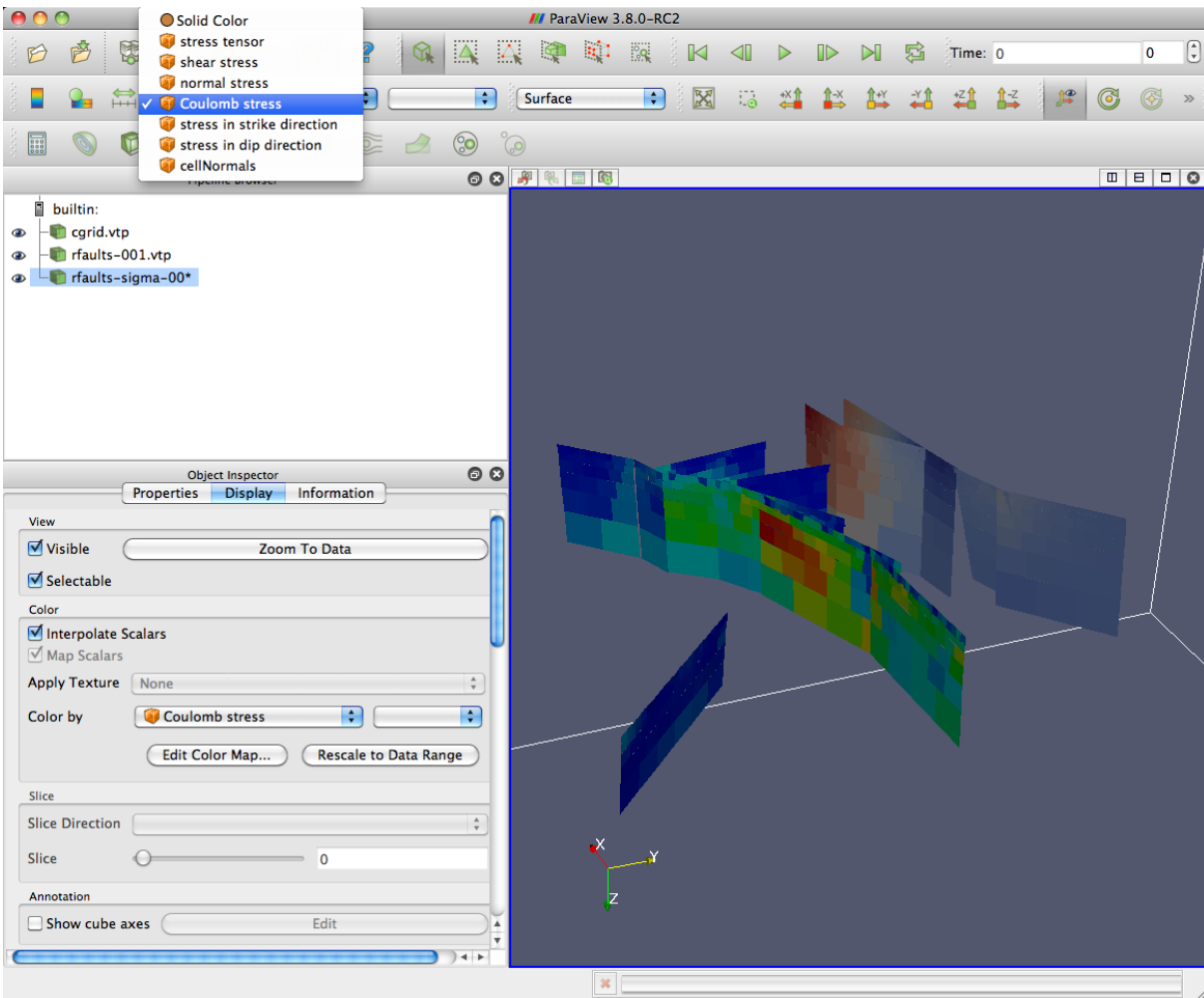


Figure 15: Load the receiver faults, in the case the Hector Mine ruptured faults, and color by one in: shear, normal, Coulomb, strike-direction shear, dip-direction shear stresses. Rescale to data range in the “Display” window, if necessary.

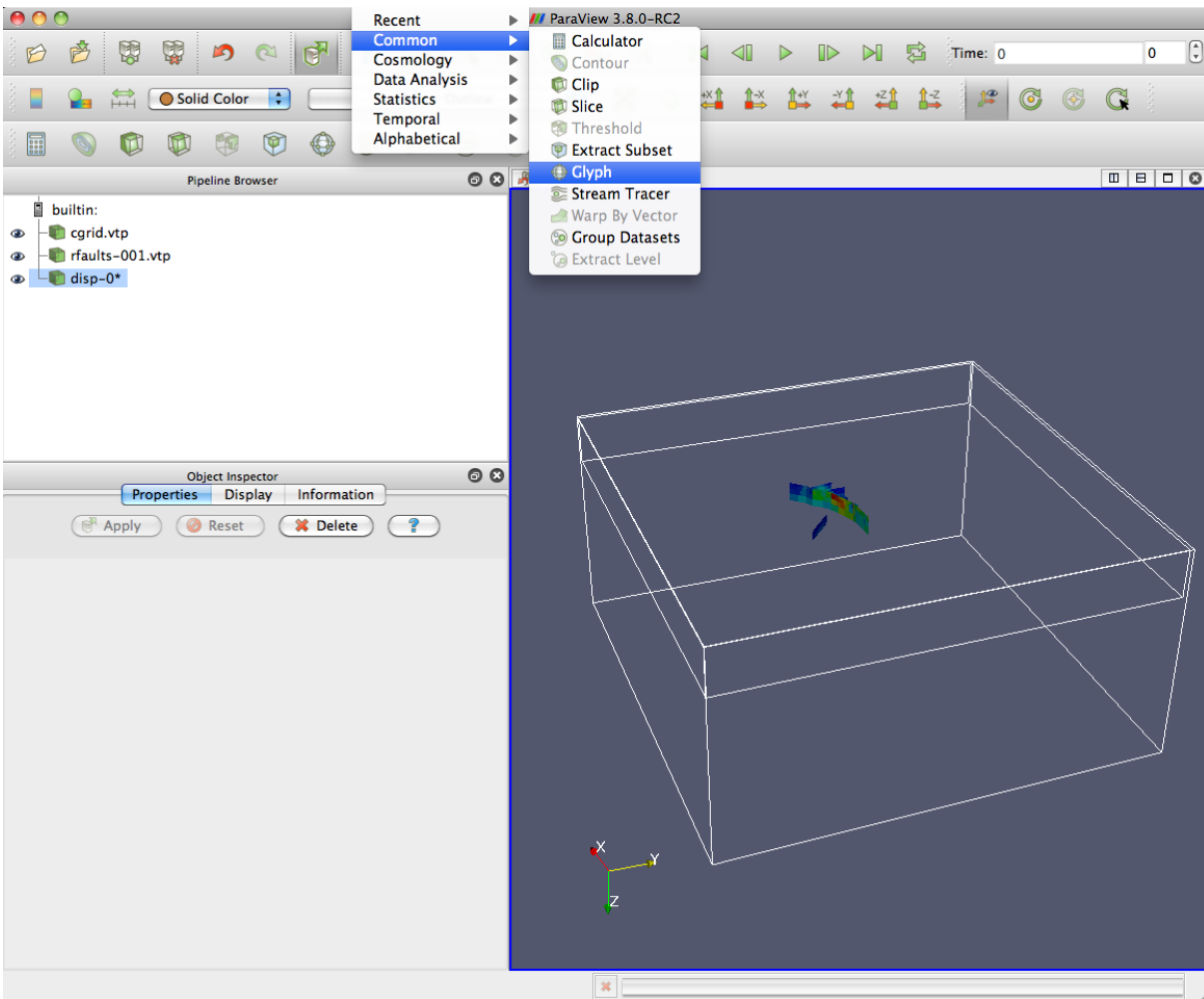


Figure 16: Load the displacement field (disp-0* appears on the “Pipeline Browser”) and apply the “Glyph” filter.

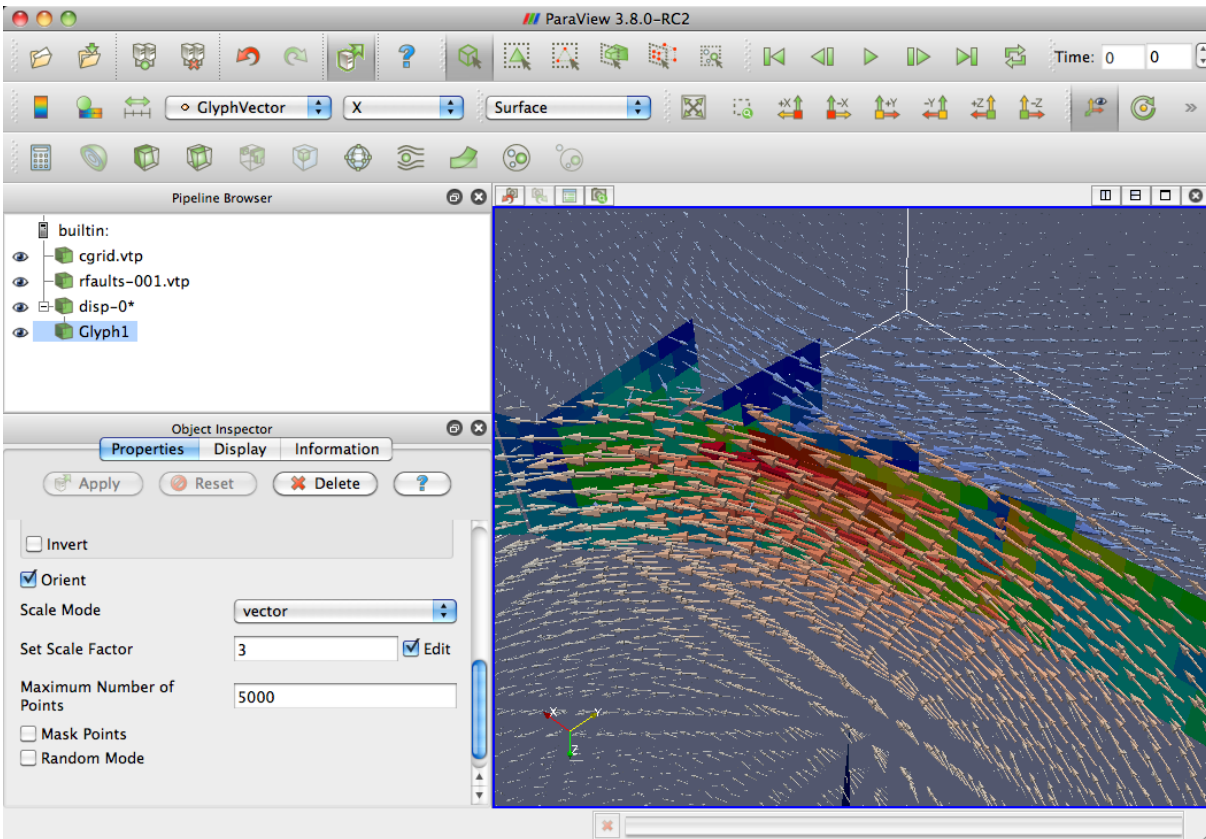


Figure 17: Adjust the scale factor, points masking and random mode and set the color to “GlyphVector”.

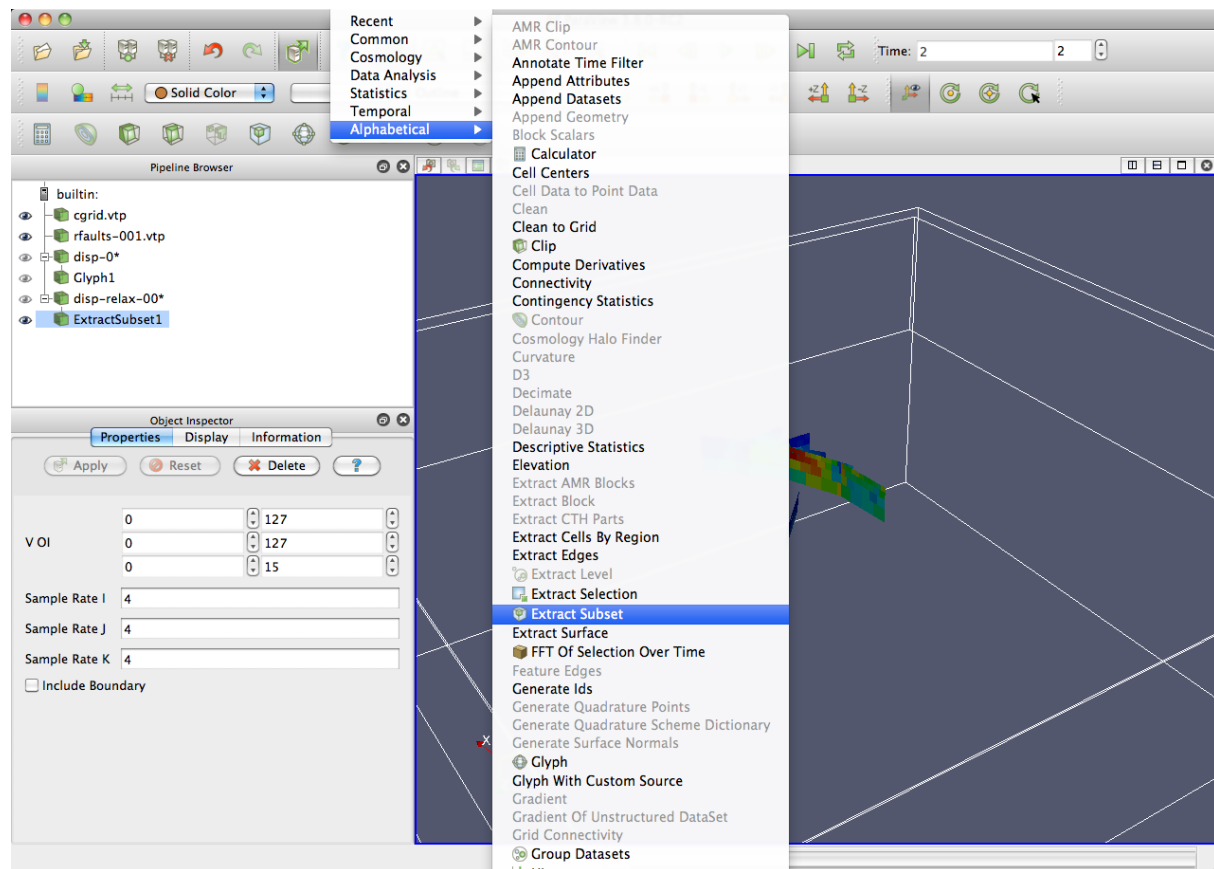


Figure 18: Load the relaxation component of the deformation (“disp-relax-0*” appears on the “Pipeline Browser”), then decimate the data set to prepare for a larger displacement field vector. To take one every four points, adjust the “Sample Rate I” accordingly.

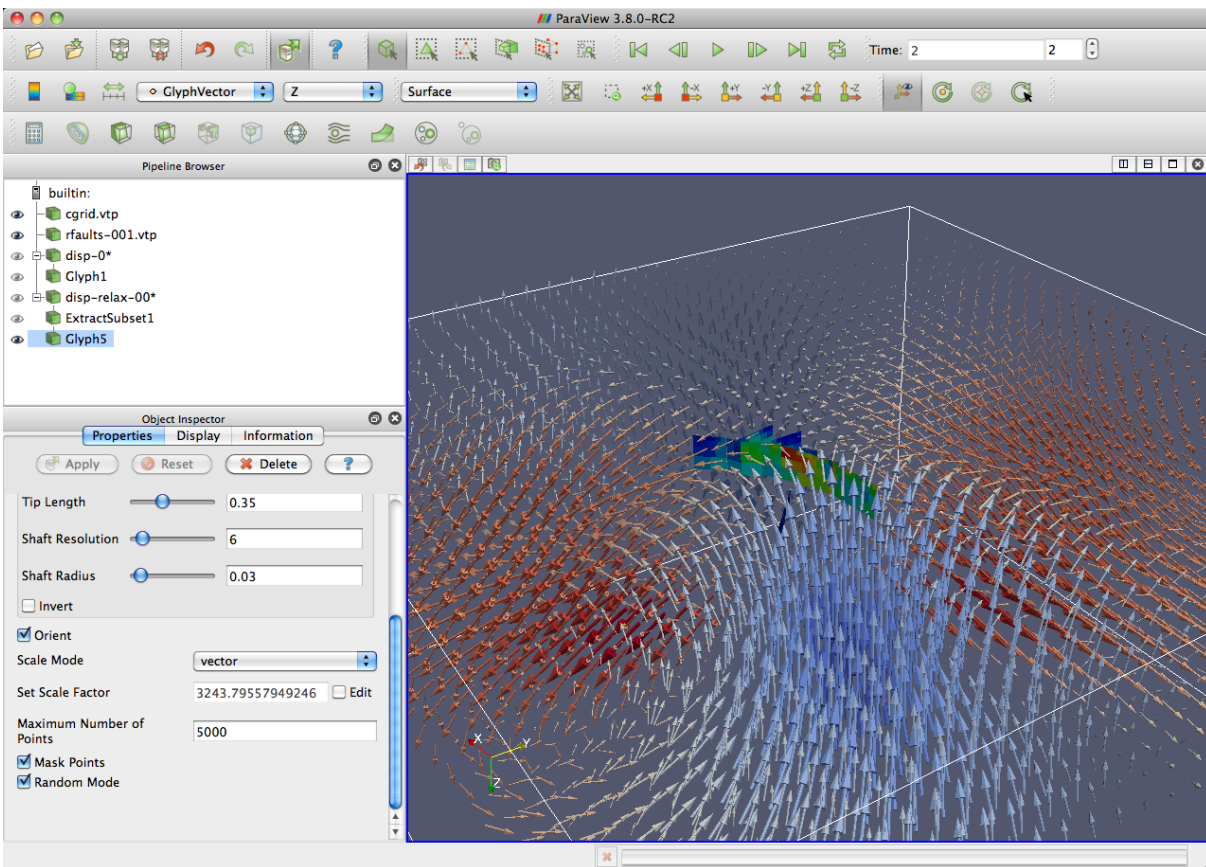


Figure 19: Apply the “Glyph” filter on the “ExtractSubset1” new data set, then change the color scale to “GlyphVector” and cancel the visibility of the “ExtractSubset1”, the “disp-relax-00*” datasets (check out the eye controls).

- Barbot, S., Y. Fialko, and D. Sandwell, Three-Dimensional Models of Elasto-Static Deformation in Heterogeneous Media, with Applications to the Eastern California Shear Zone, *Geophys. J. Int.*, 179(1), 500–520, 2009b.
- Béjar-Pizarro, M., et al., Asperities and barriers on the seismogenic zone in North Chile: state-of-the-art after the 2007 Mw 7.7 Tocopilla earthquake inferred by GPS and InSAR data, *Geophys. J. Int.*, 181(1), 390–406, 2010.
- Beroza, G. C., Near-source modeling of the Loma Prieta earthquake: Evidence for heterogeneous slip and implications for earthquake hazard, *Bull. Seism. Soc. Am.*, 81, 1603–1621, 1991.
- Bruhat, L., S. Barbot, and J. P. Avouac, Evidence for postseismic deformation of the lower crust following the 2004 Mw6.0 Parkfield earthquake, *J. Geophys. Res.*, 116, 10, 2011.
- Chlieh, M., et al., Coseismic Slip and Afterslip of the Great Mw 9.15 Sumatra-Andaman Earthquake of 2004, *Bull. Seism. Soc. Am.*, 97(1A), S152–S173, doi:10.1785/0120050631, 2007.
- Elliott, J. R., R. J. Walters, P. C. England, J. A. Jackson, Z. Li, and B. Parsons, Extension on the Tibetan plateau: recent normal faulting measured by InSAR and body wave seismology, *Geophys. J. Int.*, 183(2), 503–535, 2010.
- Elliott, J. R., E. K. Nissen, P. C. England, J. A. Jackson, S. Lamb, Z. Li, M. Oehlers, and B. Parsons, Slip in the 2010–2011 Canterbury earthquakes, New Zealand, *J. Geophys. Res.*, 117(B03401), 36, 2012.
- Fialko, Y., Evidence of fluid-filled upper crust from observations of post-seismic deformation due to the 1992 M_w 7.3 Landers earthquake, *J. Geophys. Res.*, 109, B08,401, 10.1029/2004JB002,985, 2004.
- Hudnut, K. W., et al., Co-seismic displacements of the 1994 Northridge, California, Earthquake, *Bull. Seism. Soc. Am.*, 86(1b), S19–S36, 1996.
- Johnson, J. M., K. Satake, S. R. Holdahl, and J. Sauber, The 1964 Prince William Sound earthquake: Joint inversion of tsunami and geodetic data, *J. Geophys. Res.*, 101(B1), 523–532, 1996.
- Johnson, K. M., Y. J. Hsu, P. Segall, and S. B. Yu, Fault geometry and slip distribution of the 1999 chi-chi, taiwan earthquake imaged from inversion of gps data, *Geophys. Res. Lett.*, 28(11), 2285–2288, 2001.
- Konca, A. O., V. Hjorleifsdottir, A. Song, J.-P. Avouac, D. V. Helmberger, C. Ji, K. Sieh, R. Briggs, and A. Meltzner, Rupture kinematics of the 2005, Mw 8.6, Nias- Simeulue earthquake from the joint inversion of seismic and geodetic data, *Bull. Seism. Soc. Am.*, 97(1A), S307–S322, 2007.
- Lasserre, C., G. Peltzer, F. Crampé, Y. Klinger, J. V. der Woerd, and P. Tapponnier, Coseismic deformation of the 2001 Mw = 7.8 Kokoxili earthquake in Tibet, measured by synthetic aperture radar interferometry, *J. Geophys. Res.*, 110(B12408), 17, 2005.
- Li, Z., J. R. Elliott, W. Feng, J. A. Jackson, B. E. Parsons, and R. J. Walters, The 2010 MW 6.8 Yushu (Qinghai, China) earthquake: Constraints provided by InSAR and body wave seismology, *J. Geophys. Res.*, 116(B10302), 16, 2011.
- Lorito, S., F. Romano, S. Atzori, X. Tong, A. Avallone, J. McCloskey, M. Cocco, E. Boschi, and A. Piatanesi, Limited overlap between the seismic gap and coseismic slip of the great 2010 Chile earthquake, *Nature Geoscience*, 4, 173–177, 2011.
- Luttrell, K. M., X. Tong, D. T. Sandwell, B. A. Brooks, and M. G. Bevis, Estimates of stress drop and crustal tectonic stress from the 27 February 2010 Maule, Chile, earthquake: Implications for fault strength, *J. Geophys. Res.*, 116(B11), 2011.
- Mogi, K., Relations between the eruptions of various volcanoes and the deformations of the ground surfaces around them, *Bull. Earthquake Res. Inst. Univ. Tokyo*, 36, 99–134, 1958.

- Okada, Y., Internal deformation due to shear and tensile faults in a half-space, *Bull. Seism. Soc. Am.*, 82, 1018–1040, 1992.
- Rousset, B., S. Barbot, J. P. Avouac, and Y.-J. Hsu, Postseismic Deformation Following the 1999 Chi-Chi Earthquake, Taiwan: Implication for Lower-Crust Rheology, *J. Geophys. Res.*, 117(B12405), 16, 2012.
- Ryder, I., R. Bürgmann, and F. Pollitz, Lower crustal relaxation beneath the Tibetan Plateau and Qaidam Basin following the 2001 Kokoxili earthquake, *Geophys. J. Int.*, 187, 613–630, 2011.
- Simons, M., Y. Fialko, and L. Rivera, Coseismic deformation from the 1999 M_w 7.1 Hector Mine, California, earthquake, as inferred from InSAR and GPS observations, *Bull. Seism. Soc. Am.*, 92, 1390–1402, 2002.
- Song, S. G., G. C. Beroza, and P. Segall, A unified source model for the 1906 San Francisco earthquake, *Bull. Seism. Soc. Am.*, 98, 823–831, 2008.
- Steblov, G. M., N. F. Vasilenko, A. S. Prytkov, D. I. Frolov, and T. A. Grekova, Dynamics of the Kuril-Kamchatka subduction zone from GPS data, *Izvestiya, Phys. Solid Earth*, 46(5), 440–445, 2010.
- Thomas, M. Y., J.-P. Avouac, J. Champenois, J.-C. Lee, and L.-C. Kuo, Spatiotemporal evolution of seismic and aseismic slip on the Longitudinal Valley Fault, Taiwan, *J. Geophys. Res.*, 2014.
- Tong, X., D. T. Sandwell, and Y. Fialko, Coseismic slip model of the 2008 Wenchuan earthquake derived from joint inversion of interferometric synthetic aperture radar, GPS, and field data, *J. Geophys. Res.*, 115(B4), 19, 2011.
- Wang, R., F. Martin, and F. Roth, Computation of deformation induced by earthquakes in a multi-layered elastic crust - FORTRAN programs EDGRN/EDCMP, *Comp. Geosci.*, 29, 195–207, 2003.
- Wang, R., F. Lorenzo-Martin, and F. Roth, PSGRN/PSCMP-a new code for calculating co- and post-seismic deformation, geoid and gravity changes based on the viscoelastic-gravitational dislocation theory, *Computers and Geosciences*, 32, 527–541, 2006.
- Wei, S., R. Graves, D. Helmberger, J.-P. Avouac, and J. Jiang, Sources of shaking and flooding during the Tohoku-Oki earthquake: A mixture of rupture styles, *Earth Planet. Sc. Lett.*, 333-334, 91–100, 2012.
- Wei, S., D. Helmberger, and J.-P. Avouac, Modeling the 2012 Wharton basin earthquakes off-Sumatra: Complete lithospheric failure, *J. Geophys. Res.*, 118(7), 3592–3609, 2013.
- Wei, S., et al., Superficial simplicity of the 2010 El Mayor-Cucapah earthquake of Baja California in Mexico, *Nature Geosci.*, pp. 615–618, 2011.
- Yamazaki, Y., T. Lay, K. F. Cheung, H. Yue, and H. Kanamori, Modeling near-field tsunami observations to improve finite-fault slip models for the 11 March 2011 Tohoku earthquake, *Geophys. Res. Lett.*, 38(7), 2011.